

Structure-Preserving Numerical Methods for Nonlinear Fokker–Planck Equations with Nonlocal Interactions by an Energetic Variational Approach

Chenghua Duan* Wenbin Chen† Chun Liu‡ Xingye Yue§ Shenggao Zhou¶

August 18, 2020

Abstract

In this work, we develop novel structure-preserving numerical schemes for a class of nonlinear Fokker–Planck equations with nonlocal interactions. Such equations can cover many cases of importance, such as porous medium equations with external potentials, optimal transport problems, and aggregation-diffusion models. Based on the Energetic Variational Approach, a trajectory equation is first derived by using the balance between the maximal dissipation principle and least action principle. By a convex-splitting technique, we propose energy dissipating numerical schemes for the trajectory equation. Rigorous numerical analysis reveals that the nonlinear numerical schemes are uniquely solvable, naturally respect mass conservation and positivity at fully discrete level, and preserve steady states. Under certain smoothness assumptions, the numerical schemes are shown to be second order accurate in space and first order accurate in time. Extensive numerical simulations are performed to demonstrate several valuable features of the proposed schemes. In addition to the preservation of physical structures, such as positivity, mass conservation, discrete energy dissipation, blue and steady states, numerical simulations further reveal that our numerical schemes are capable of solving *degenerate* cases of the Fokker–Planck equations effectively and robustly. It is shown that the developed numerical schemes have convergence order even in degenerate cases with the presence of solutions having compact support, can accurately and robustly compute the waiting time of free boundaries without any oscillation, and can approximate blow-up singularity up to machine precision.

Keywords: Nonlocal Fokker–Planck Equations; Positivity; Energy Dissipation; Degeneracy; Waiting Time

AMS Subject Classifications: 35K65; 76M28; 76M20; 82Cxx

*Shanghai Center for Mathematical Sciences, Fudan University, Shanghai 200438, China. Email: chduan@fudan.edu.cn.

†School of Mathematical Sciences and Shanghai Key Laboratory for Contemporary Applied Mathematics, Fudan University, Shanghai 200433, China. Email: wbchen@fudan.edu.cn.

‡Department of Applied Mathematics, Illinois Institute of Technology, Chicago, IL 60616, USA. Email: cliu124@iit.edu.

§Department of Mathematics and Mathematical Center for Interdiscipline Research, Soochow University, Suzhou 215006, Jiangsu, China. Email: xyyue@suda.edu.cn.

¶Corresponding author. Department of Mathematics and Mathematical Center for Interdiscipline Research, Soochow University, Suzhou 215006, Jiangsu, China. Email: sgzhou@suda.edu.cn.

1 Introduction

We focus on the following initial-boundary value problem

$$\begin{cases} \partial_t u = \partial_x \{f(u) \partial_x [H'(u) + V(x) + W * u]\}, & x \in \Omega, t > 0, \\ u(x, 0) = u_0(x), & x \in \Omega, \\ f(u) \partial_x [H'(u) + V(x) + W * u] = 0, & x \in \partial\Omega, t > 0, \end{cases} \quad (1.1)$$

where $u(x, t) \geq 0$ represents the time-dependent probability density, $\Omega \subset \mathbb{R}$ is a bounded domain, $H(\cdot) : \mathbb{R}^+ \cup \{0\} \rightarrow \mathbb{R}$ is the density of internal energy with $H''(\cdot) > 0$, $V(\cdot)$ is an external potential, $W(\cdot)$ is an even Lipschitz continuous function describing particle interactions, and $f : \mathbb{R}^+ \cup \{0\} \rightarrow \mathbb{R}^+ \cup \{0\}$ is a given increasing differentiable function with $f(0) = 0$ and $f'(0) \neq 0$.

The Fokker-Planck (FP) equation in the problem (1.1) arises from various applications. Such an equation can be derived as mean-field limits of particle systems and has been used in various models to describe interacting gases [14, 51], granular materials [6], collective motion of animals [49, 32, 16], and cell migration and chemotaxis phenomena in biology [20, 37, 11]. The FP equation covers many cases of importance. For instance, when $f(u) = u$, $V = W = 0$, and $H'(u) = u^m (m > 1)$, it becomes the porous medium equation [13]. When considering a nonzero nonlocal interaction term, i.e., $W \neq 0$, it is referred as the nonlocal FP equation [17, 35, 42]. Typical interaction potentials, $W(\cdot)$, appearing in above applications include fully attractive cases, such as the Newtonian or Bessel potentials in chemotaxis [20] and power-laws in granular materials [14]; cases that are repulsive in the short range and attractive in the long range, such as combinations of power-law potentials and Morse-type potentials in swarming [15, 49]; and cases with compactly supported potentials in many biological applications, such as networks and cell sorting [4, 10, 20].

Mathematically, any solution to the problem (1.1) has three main properties

- Non-negativity: if $u_0(x) \geq 0$, then $u(x, t) \geq 0, \forall x \in \Omega, t > 0$;
- Mass conservation: $\int_{\Omega} u_0(x) dx = \int_{\Omega} u(x, t) dx$;
- Energy dissipation:

$$\frac{d}{dt} E^{total} = -\Delta \leq 0, \quad (1.2)$$

where

$$E^{total} := \int_{\Omega} H(u(x)) dx + \int_{\Omega} u(x) V(x) dx + \frac{1}{2} \int_{\Omega} \int_{\Omega} W(x-y) u(x) u(y) dy dx,$$

and

$$\Delta = \int_{\Omega} f(u) |\partial_x [H'(u) + V(x) + W * u]|^2 dx.$$

The property (1.2) has played a critical role in analyzing the dynamics of the problem (1.1) in the works [12, 14, 51, 48]. Therefore, it is crucial and highly desirable to develop numerical methods that are able to maintain an analogous energy dissipation in the discrete sense. Another challenge to obtain physically faithful numerical solutions lies in the development of numerical schemes that can guarantee the non-negativity of the numerical density while retaining the mass conservation, especially in the degenerate case. Recently, various numerical schemes addressing

above concerns, ranging from finite volume methods to discontinuous Galerkin (DG) methods, have been developed to numerically solve the FP type of equations in the literature. Finite volume schemes with second order accuracy have been proposed for the problem (1.1) in [7, 17]. The schemes have semi-discrete (in space) entropy dissipation and positivity preserving properties for explicit-in-time discretization under a restriction on time step size due to the Courant–Friedrichs–Lewy (CFL) condition. Entropic schemes have been developed in [9] to solve the FP equations for a simplified model of granular media. It has been proved that the entropic schemes have many attractive properties, such as mass conservation, entropy decay, and positivity and equilibrium preserving. Based on entropic average fluxes, another type of entropic schemes have been constructed to solve the nonlocal, nonlinear FP equations [41]. It also has been shown that the constructed entropic schemes are able to preserve positivity, semi-discrete entropy dissipation, and asymptotic steady states with arbitrary accuracy. The work [35] has proposed high order direct DG schemes, in which a discrete version of entropy dissipation law is respected by numerical solutions and positivity is enforced by a delicate reconstruction algorithm that is able to maintain accuracy. To achieve high order accuracy, high order DG schemes for (1.1) have been established in the work [48]. For an interaction potential with a smooth kernel, the proposed semi-discrete DG scheme admits an entropy inequality at discrete level. The fully discretized DG scheme is able to produce non-negative solutions under a time step size constraint, with the help of a positivity-preserving limiter. Based on harmonic-mean approximations, finite difference schemes that are proved to respect mass conservation and unconditional positivity preservation have been proposed in [42]. Estimates on the condition number of the coefficient matrix has been established as well. More recently, a fully discrete, implicit-in-time finite volume scheme that ensures the positivity and energy-decaying properties has been established in the work [3].

Another closely related model, the Poisson–Nernst–Planck (PNP) equations, can be regarded as the problem (1.1) with $f(u) = u$, $H(u) = u \log u$, and a nonlocal Coulombic interaction kernel that is coupled through a Poisson equation. Related numerical methods [44, 45, 43, 46] with structure-preserving properties for the PNP equations can be extended to numerically solve the the problem (1.1) as well. There are other types of numerical methods for the nonlocal case, e.g., particle methods [19] and evolving diffeomorphisms methods [18]. However, energy dissipation law in fully discrete level and convergence order of numerical schemes have not been well studied. In addition to above structure-preserving features at fully discrete level, it is rather challenging to develop numerical schemes that can capture finite-speed propagation and possible waiting time in degenerate cases. For solutions with compact support, it is non-trivial to show the convergence order, even numerically. When a solution blows up in a finite time, the standard finite difference methods, finite volume schemes, or DG methods, only present the order of $\mathcal{O}(1/h)$ blow-up on an equidistant mesh with grid spacing h . Improvement addressing these issues is still in lack.

In this paper, we propose a novel numerical scheme based on an Energetic Variational Approach (EnVarA), which is a balance between the maximal dissipation principle (MDP) and least action principle (LAP). The approach was originated from a pioneering work due to Onsager [39, 40] and further improved by Strutt [47]. In recent years, it has been applied to develop mathematical models for complex physical systems [33, 30, 22, 28], as well as numerical schemes for porous medium equations [24] and the Wright-Fisher model that describes genetic drift [23]. We first derive a trajectory equation and then establish its numerical scheme by a convex splitting technique. The positivity and mass conservation of the numerical solution can be preserved naturally. Numerical analysis proves that the numerical scheme is uniquely solvable, satisfies a

discretized energy dissipation law, and preserves steady states. The proposed numerical scheme for the trajectory equation can also be justified at theoretical level that the convergence rate is first order in time and second in space. We conduct extensive numerical tests to demonstrate several valuable advantages of the proposed schemes in overcoming the difficulties in the development of numerical methods for the FP equations. In addition to the success in preservation of physical structures, including positivity, mass conservation, discrete energy dissipation, and steady states, our numerical simulations further demonstrate that the proposed schemes are able to solve the *degenerate* FP equations effectively and robustly. Numerical results reveal that the developed numerical schemes have convergence order even in degenerate cases with the presence of solutions having compact support, can accurately and robustly calculate the waiting time of free boundaries without any oscillation, and can simulate blow-up singularity up to machine precision.

This paper is organized as follows. The EnVarA and trajectory equation of the nonlinear Fokker–Planck equations are outlined in Section 2. The numerical scheme is described in Section 3. Subsequently, the proof of unique solvability, energy stability, optimal rate convergence analysis and steady-state preserving is provided in Section 4. Section 5 presents various numerical results. Finally, in Section 6, we draw conclusions.

2 Energetic Variational Approach

We first introduce the Lagrangian and Eulerian coordinate systems.

Definition 2.1. *Suppose that Ω_0^X and $\Omega_t^x \subset \mathbb{R}^m$, $m \in \mathbb{N}^+$, are domains with smooth boundaries, time $t > 0$, and \mathbf{v} is a smooth vector field in \mathbb{R}^m . The flow map $x(X, t) : \Omega_0^X \rightarrow \Omega_t^x$ is defined as a solution of*

$$\begin{cases} \frac{d}{dt}x(X, t) = \mathbf{v}(x(X, t), t), & t > 0, \\ x(X, 0) = X, \end{cases} \quad (2.1)$$

where $X = (X_1, \dots, X_m) \in \Omega_0^X$ and $x = (x_1, \dots, x_m) \in \Omega_t^x$. The coordinate system X is called the Lagrangian coordinate and Ω_0^X is called the reference configuration; the coordinate system x is called the Eulerian coordinate and Ω_t^x is called the deformed configuration.

Since Ω_0^X and Ω_t^x are the same domain described by different coordinate systems, we denote the domain under consideration uniformly by Ω in the rest of this paper. Also, we assume that the Jacobian of the flow map, $\det \frac{\partial x(X, t)}{\partial X}$, remains positive in time evolution.

Now we derive a trajectory equation for the nonlinear nonlocal Fokker–Planck equations. The initial-boundary value problem (1.1) is equivalent to

$$\begin{cases} \partial_t u + \partial_x(u\mathbf{v}) = 0, & x \in \Omega, t > 0, \\ \mathbf{v} = -\frac{f(u)}{u} \partial_x[H'(u) + V(x) + W * u], & x \in \Omega, \\ u(x, 0) = u_0(x) > 0, & x \in \Omega, \\ f(u) \partial_x \{ [H'(u) + V(x) + W * u] \} \Big|_{\partial\Omega} = 0, & t > 0, \end{cases} \quad (2.2)$$

where \mathbf{v} is the velocity. It is well-defined as u goes to zero, by the assumption that $f(0) = 0$ and $f'(0) \neq 0$.

Lemma 2.2. *If $u(x, t)$ is the solution of (1.1), then u satisfies the corresponding energy dissipation law*

$$\frac{d}{dt} E^{total} = -\Delta, \quad (2.3)$$

where the total energy

$$E^{total} := \int_{\Omega} [H(u) + uV(x)] dx + \frac{1}{2} \int_{\Omega} \int_{\Omega} W(x-y) u(x) u(y) dy dx,$$

and the entropy production

$$\Delta = \int_{\Omega} \frac{u^2}{f(u)} |\mathbf{v}|^2 dx,$$

with the velocity $\mathbf{v} = -\frac{f(u)}{u} \partial_x [H'(u) + V(x) + W * u]$. If u satisfies the corresponding energy dissipation law (2.3) and a zero-flux boundary condition, then it can be shown by the Energetic Variational Approach that $u(x, t)$ solves (1.1).

Proof: We first prove that the energy dissipation law (2.3) holds if u is the solution of (2.2). Multiplying by $H'(u) + V(x) + W * u$ and integrating on both sides of the first equation in (2.2), we have

$$\int_{\Omega} [H'(u) + V(x) + W * u] \cdot \partial_t u dx = - \int_{\Omega} \partial_x (u\mathbf{v}) \cdot [H'(u) + V(x) + W * u] dx.$$

By integration by parts, we have

$$\frac{d}{dt} E^{total} = \int_{\Omega} u\mathbf{v} \cdot \{\partial_x [H'(u) + V(x) + W * u]\} dx = - \int_{\Omega} \frac{u^2}{f(u)} |\mathbf{v}|^2 dx,$$

where the velocity $\mathbf{v} = -\frac{f(u)}{u} \partial_x [H'(u) + V(x) + W * u]$ and we have used the zero-flux boundary condition $u\mathbf{v}|_{\partial\Omega} = 0$; cf. the system (2.2).

Next we shall show by the EnVarA that (2.2) can be deduced from the energy dissipation law (2.3). By mass conservation, we have

$$0 = \frac{d}{dt} \int_{E_t^x} u(x, t) dx = \frac{d}{dt} \int_{E_0^X} u(x(X, t), t) \det \frac{\partial x}{\partial X} dX = \int_{E_t^x} u_t + \partial_x u \cdot \mathbf{v} + u(x, t) \cdot \partial_x \mathbf{v} dx,$$

where \mathbf{v} denotes the velocity, $E_t^x \subset \Omega_t^x$ is the deformed configuration of an arbitrary subdomain $E_0^X \subset \Omega_0^X$, and $\det \frac{\partial x(X, t)}{\partial X}$ is the Jacobian matrix of the map: $X \rightarrow x(X, t)$. Thus, we have

$$u_t + \partial_x (u\mathbf{v}) = 0. \quad (2.4)$$

In the Lagrangian coordinate, mass conservation leads to

$$u(x(X, t), t) = \frac{u_0(X)}{\det \frac{\partial x(X, t)}{\partial X}}, \quad (2.5)$$

where $u_0(X)$ is the initial condition.

- **Least Action Principle.** The action functional is defined as

$$\begin{aligned} \mathcal{A}(x) := & - \int_0^{t^*} \int_{\Omega} H\left(\frac{u_0(X)}{\partial_X x}\right) \partial_X x \, dX dt - \int_0^{t^*} \int_{\Omega} u_0(X) V(x) dX dt \\ & - \frac{1}{2} \int_0^{t^*} \int_{\Omega} \int_{\Omega} u_0(X) u_0(Y) W(x-y) dX dY dt, \end{aligned} \quad (2.6)$$

where t^* is a positive number denoting the time period under consideration.

Based on the Least Action Principle, we have the conservative force in the Eulerian coordinate by taking the variational of $\mathcal{A}(x, t)$ with respect to x :

$$F_{con} := \frac{\delta \mathcal{A}}{\delta x} = -u \partial_x [H'(u) + V(x) + W * u].$$

In the Lagrangian coordinate, we have

$$F_{con} = -\partial_X \left[\frac{u_0(X)}{\partial_X x} \cdot H' - H \right] - u_0(X) V'(x) - u_0(X) \mathcal{S}(x),$$

where

$$\mathcal{S}(x) := \int_{\Omega} W'(x(X, t) - y(Y, t)) u_0(Y) dY. \quad (2.7)$$

- **Maximum Dissipation Law.** By the Maximum Dissipation Law, i.e., the Onsager's Principle, we obtain the dissipation force by taking the variation of $\frac{1}{2}\Delta$ with respect to the velocity \mathbf{v} :

$$F_{dis} := \frac{\delta(\frac{1}{2}\Delta)}{\delta \mathbf{v}}.$$

Here the factor $\frac{1}{2}$ is included according to the convention that the energy dissipation Δ is always a quadratic function of certain rates, such as the velocity in the linear response theory [47].

We obtain the dissipation force

$$F_{dis} = \frac{u^2}{f(u)} \mathbf{v} \quad (2.8)$$

and

$$F_{dis} = \frac{u_0^2(X)}{\partial_X x} \cdot \frac{1}{f\left(\frac{u_0(X)}{\partial_X x}\right)} \cdot x_t$$

in the Eulerian coordinate and Lagrangian coordinate, respectively.

- **Force Balance.** By the Newton's force balance law $F_{con} = F_{dis}$, we have the trajectory equation

$$\frac{u_0^2(X)}{\partial_X x} \cdot \frac{1}{f\left(\frac{u_0(X)}{\partial_X x}\right)} \cdot x_t = -\partial_X \left[\frac{u_0(X)}{\partial_X x} H'\left(\frac{u_0(X)}{\partial_X x}\right) - H\left(\frac{u_0(X)}{\partial_X x}\right) \right] - u_0(X) V'(x) - u_0(X) \mathcal{S}(x), \quad (2.9)$$

in the Lagrangian coordinate, where $\mathcal{S}(x)$ is given in (2.7). In the Eulerian coordinate, we have

$$\frac{u^2}{f(u)}\mathbf{v} = -u\partial_x [H' + V(x) + W * u]. \quad (2.10)$$

Thus, we have by (2.10) that the velocity $\mathbf{v} = -\frac{f(u)}{u}\partial_x[H'(u) + V(x) + W * u]$. Combination of (2.4), (2.10), and the zero-flux boundary condition completes the proof. \square

The trajectory $x(X, t)$ is obtained by solving (2.9) with the initial condition

$$x(X, 0) = X, \quad X \in \Omega, \quad (2.11)$$

and the boundary condition

$$x|_{\partial\Omega} = X|_{\partial\Omega}, \quad t > 0. \quad (2.12)$$

With the flow map $x(X, t)$, we obtain the solution $u(x, t)$ to the problem (1.1) by the equation (2.5).

Remark 2.3. Notice that the initial condition $u_0(X) > 0$ on Ω is considered in Lemma 2.2. The case with compactly supported initial conditions will be treated as free boundary problems in Section 3.

3 Numerical Methods for Trajectory Equation

In this section, we propose a structure-preserving finite difference scheme for the trajectory equation (2.9).

3.1 Time Discretization

We develop a time discretization scheme using the convex splitting strategy. It follows from the convexity of $H(u)$ that the term $H\left(\frac{u_0}{\partial_X x}\right)\partial_X x$ is convex as well, by the assumption that $\partial_X x > 0$. The functions $V(x)$ and $W(x)$ in (1.2) can be split into convex part and concave part, i.e.,

$$V(x) := V_c(x) - V_e(x),$$

$$W(x) := W_c(x) - W_e(x),$$

where $V_c, W_c, V_e,$ and W_e are convex functions. Then the trajectory equation (2.9) can be viewed as a gradient flow associated with the total energy

$$\begin{aligned} E^{total} &= \int_{\Omega} H\left(\frac{u_0(X)}{\partial_X x}\right)\partial_X x + u_0(X)V(x)dX + \frac{1}{2}\int_{\Omega}\int_{\Omega} W(x-y)u_0(X)u_0(Y)dXdY \\ &:= E_c^{total} - E_e^{total}, \end{aligned} \quad (3.1)$$

where

$$E_c^{total} := \int_{\Omega} H\left(\frac{u_0(X)}{\partial_X x}\right)\partial_X x + u_0(X)V_c(x)dX + \frac{1}{2}\int_{\Omega}\int_{\Omega} W_c(x-y)u_0(X)u_0(Y)dXdY,$$

and

$$E_e^{total} := \int_{\Omega} u_0(X) V_e(x) dX + \frac{1}{2} \int_{\Omega} \int_{\Omega} W_e(x-y) u_0(X) u_0(Y) dX dY.$$

Notice that both E_e^{total} and E_c^{total} are convex functionals with respect to the trajectory $x(X)$.

Based on a convex splitting technique [29, 23], we propose a *semi-discrete scheme* for (1.1):

$$\begin{aligned} \frac{u_0^2(X)}{\partial_X x^n} \cdot \frac{1}{f\left(\frac{u_0(X)}{\partial_X x^n}\right)} \cdot \frac{x^{n+1} - x^n}{\tau} = & -\partial_X \left[\frac{u_0(X)}{\partial_X x^{n+1}} \cdot H' \left(\frac{u_0(X)}{\partial_X x^{n+1}} \right) - H \left(\frac{u_0(X)}{\partial_X x^{n+1}} \right) \right] \\ & - u_0(X) V_c'(x^{n+1}) - u_0(X) V_e'(x^n) - u_0(X) \mathcal{S}_c^{n+1} + u_0(X) \mathcal{S}_e^n, \end{aligned}$$

where $\tau := \frac{T}{N}$, $N \in \mathbb{N}^+$, is the time step size with the final time T , and

$$\mathcal{S}_c^{n+1} := \int_{\Omega} W_c'(x^{n+1} - y^{n+1}) u_0(Y) dY$$

and

$$\mathcal{S}_e^n := \int_{\Omega} W_e'(x^n - y^n) u_0(Y) dY.$$

3.2 Fully Discrete Scheme with a Positive Initial State

Let X_0 be the left endpoint of Ω and $h = \frac{|\Omega|}{M}$ be the mesh step with $M \in \mathbb{N}^+$. Denote by $X_r = X(r) = X_0 + rh$, where r takes integer or half integer values. Let \mathcal{E}_M and \mathcal{C}_M be the spaces of grid functions whose domains are $\{X_i \mid i = 0, \dots, M\}$ and $\{X_{i-\frac{1}{2}} \mid i = 1, \dots, M\}$, respectively. In componentwise, these functions are identified via $l_i = l(X_i)$, $i = 0, \dots, M$, for $l \in \mathcal{E}_M$, and $\phi_{i-\frac{1}{2}} = \phi(X_{i-\frac{1}{2}})$, $i = 1, \dots, M$, for $\phi \in \mathcal{C}_M$. Without ambiguity, we denote by $X = \{X_i \mid i = 0, \dots, M\}$ for $X \in \mathcal{E}_M$.

We define difference operators $D_h : \mathcal{E}_M \rightarrow \mathcal{C}_M$, $d_h : \mathcal{C}_M \rightarrow \mathcal{E}_M$, and $\tilde{D}_h : \mathcal{E}_M \rightarrow \mathcal{E}_M$ by

$$(D_h l)_{i-\frac{1}{2}} = (l_i - l_{i-1})/h, \quad i = 1, \dots, M, \quad (3.2)$$

$$(d_h \phi)_i = (\phi_{i+\frac{1}{2}} - \phi_{i-\frac{1}{2}})/h, \quad i = 1, \dots, M-1, \quad (3.3)$$

$$(\tilde{D}_h l)_i = \begin{cases} (l_{i+1} - l_{i-1})/2h, & i = 1, \dots, M-1, \\ (l_{i+1} - l_i)/h, & i = 0, \\ (l_i - l_{i-1})/h, & i = M. \end{cases} \quad (3.4)$$

Let $l, g \in \mathcal{E}_M$ and $\phi, \varphi \in \mathcal{C}_M$. We define the *inner product* on space \mathcal{E}_M and \mathcal{C}_M by

$$\langle l, g \rangle_{\mathcal{E}} := h \left(\frac{1}{2} l_0 g_0 + \sum_{i=1}^{M-1} l_i g_i + \frac{1}{2} l_M g_M \right), \quad (3.5)$$

$$\langle \phi, \varphi \rangle_{\mathcal{C}} := h \sum_{i=0}^{M-1} \phi_{i+\frac{1}{2}} \varphi_{i+\frac{1}{2}}. \quad (3.6)$$

It is easy to verify the following summation by parts formula:

$$\langle l, d_h \phi \rangle_{\mathcal{E}} = -\langle D_h l, \phi \rangle_{\mathcal{C}}, \quad \text{with } l_0 = l_M = 0, \phi \in \mathcal{C}_M, l \in \mathcal{E}_M. \quad (3.7)$$

Let $\mathcal{Q} := \{l \in \mathcal{E}_M \mid l_{i-1} < l_i, 1 \leq i \leq M; l_0 = X_0, l_M = X_M\}$ be an admissible set, in which particles are arranged in the order without twisting or exchanging. Its boundary set is given by $\partial\mathcal{Q} := \{l \in \mathcal{E}_M \mid l_{i-1} \leq l_i, 1 \leq i \leq M, \text{ and exists } i_0 \in \{1, \dots, M\} \text{ such that } l_{i_0} = l_{i_0-1}; l_0 = X_0, l_M = X_M\}$. Clearly, $\bar{\mathcal{Q}} := \mathcal{Q} \cup \partial\mathcal{Q}$ is a closed convex set.

The **fully discrete scheme** is formulated as follows: Given $x^n \in \mathcal{Q}$, find $x^{n+1} = (x_0^{n+1}, \dots, x_M^{n+1}) \in \mathcal{Q}$ such that

$$\begin{aligned} \frac{u_{0_i}^2}{\widetilde{D}_h x_i^n} \cdot \frac{1}{f\left(\frac{u_{0_i}}{\widetilde{D}_h x_i^n}\right)} \cdot \frac{x_i^{n+1} - x_i^n}{\tau} = -d_h \left[\frac{u_0}{D_h x^{n+1}} \cdot H'\left(\frac{u_0}{D_h x^{n+1}}\right) - H\left(\frac{u_0}{D_h x^{n+1}}\right) \right]_i \\ - u_{0_i} V'_c(x_i^{n+1}) + u_{0_i} V'_e(x_i^n) - u_{0_i} \hat{\mathcal{S}}_{c_i}^{n+1} + u_{0_i} \hat{\mathcal{S}}_{e_i}^n, \quad 1 \leq i \leq M-1, \end{aligned} \quad (3.8)$$

with boundary conditions

$$x_0^n = X_0, \quad x_M^n = X_M. \quad (3.9)$$

Here $\hat{\mathcal{S}}_{c_i}^{n+1}$ and $\hat{\mathcal{S}}_{e_i}^n$ are given by

$$\hat{\mathcal{S}}_{c_i}^{n+1} := \langle W'_c(x_i^{n+1} - y^{n+1}), u_0(Y) \rangle_{\mathcal{E}}, \quad (3.10)$$

and

$$\hat{\mathcal{S}}_{e_i}^n := \langle W'_e(x_i^n - y^n), u_0(Y) \rangle_{\mathcal{E}}, \quad (3.11)$$

with $x_i^{n+1} := x(X_i, t^{n+1})$ and $y^{n+1} := y(Y, t^{n+1})$.

We develop a Newton's iteration method to solve the nonlinear difference equations (3.8). Define the following convex functional

$$\begin{aligned} J(z) := \frac{1}{2\tau} \left\langle \frac{u_0^2}{\widetilde{D}_h x^n} \cdot \frac{1}{f\left(\frac{u_0}{\widetilde{D}_h x^n}\right)} \cdot (z - x^n), z - x^n \right\rangle_{\mathcal{E}} + \left\langle H\left(\frac{u_0}{D_h z}\right) D_h z, \mathbf{e} \right\rangle_c \\ + \langle u_0(X), V_c(z) \rangle_{\mathcal{E}} + \frac{1}{2} \left\langle \left\langle W_c(z - y), u_0(Y) \right\rangle, u_0(X) \right\rangle_{\mathcal{E}} \\ - \langle u_0(X) V'_e(x^n), z \rangle_{\mathcal{E}} - \left\langle u_0(X) \left\langle W'_e(x^n - y^n), u_0(Y) \right\rangle, z \right\rangle_{\mathcal{E}}, \end{aligned} \quad (3.12)$$

where $x^n, y^n \in \mathcal{Q}$ are coordinates of particles at time t^n , $n = 0, \dots, N-1$, and \mathbf{e} is a vector with each element being one.

Newton's iteration. Set $x^{n+1,0} = x^n$. For $k = 0, 1, 2, \dots$, update $x^{n+1,k+1} = x^{n+1,k} + \delta_x$, where δ_x solves equations

$$\begin{aligned} \frac{u_{0_i}^2}{\widetilde{D}_h x_i^n} \cdot \frac{1}{f\left(\frac{u_{0_i}}{\widetilde{D}_h x_i^n}\right)} \cdot \frac{x_i^{n+1,k} + \delta_{x_i} - x_i^n}{\tau} \\ = -d_h \left[\frac{u_0}{D_h x^{n+1,k}} \cdot H'\left(\frac{u_0}{D_h x^{n+1,k}}\right) - H\left(\frac{u_0}{D_h x^{n+1,k}}\right) \right]_i \\ + d_h \left[\left(\frac{u_0^2}{(D_h x^{n+1,k})^3} H'' \right) D_h \delta_x \right]_i - u_{0_i} V'_c(x_i^{n+1,k}) - u_{0_i} V''_c(x_i^{n+1,k}) \delta_{x_i} \\ + u_{0_i} V'_e(x_i^n) - u_{0_i} \hat{\mathcal{S}}_{c_i}^{n+1,k} - u_{0_i} (\hat{\mathcal{S}}'_c)_i^{n+1,k} \delta_{x_i} + u_{0_i} \hat{\mathcal{S}}_{e_i}^n, \quad 1 \leq i \leq M-1, \end{aligned} \quad (3.13)$$

with boundary conditions $\delta_{x_0} = \delta_{x_M} = 0$, where

$$(\hat{\mathcal{S}}_c')_i^{n+1,k} := \left\langle W_c''(x_i^{n+1,k} - y^{n+1,k}), u_0(Y) \right\rangle_{\mathcal{E}}.$$

Remark 3.1. *To guarantee the convergence of the Newton's iterations on \mathcal{Q} theoretically, the damped Newton's iteration [38] can be used [23, 24]. However, the proposed Newton's iteration method is more efficient and converges robustly in many examples.*

After solving (3.13), we finally get numerical density $\{u_i^n\}_{i=0}^M$, $n = 1, \dots, N$, from (2.5) by

$$u_i^n = \frac{u_0(X_i)}{(x_{i+1}^n - x_{i-1}^n)/(2h)}, \quad 1 \leq i \leq M-1, \quad \text{and} \quad (3.14)$$

$$u_0^n = \frac{u_0(X_0)}{(x_1^n - x_0^n)/h}, \quad u_M^n = \frac{u_0(X_M)}{(x_M^n - x_{M-1}^n)/h}. \quad (3.15)$$

Theorem 3.2. *The numerical solution $\{u_i^n\}_{i=0}^M$, $n = 1, \dots, N$, obtained from (3.14)-(3.15), ensures mass conservation and positivity of solution with an initial condition $u_0 > 0$.*

Proof: Let the initial mass carried by each particle $x_i^0 = X_i$ be

$$m_i^0 = hu_0(X_i), \quad 1 < i < M; \quad m_0^0 = \frac{h}{2}u_0(X_0); \quad \text{and} \quad m_M^0 = \frac{h}{2}u_0(X_M). \quad (3.16)$$

Define the mass carried by each particle x_i^n as

$$m_i^n = \frac{x_{i+1}^n - x_{i-1}^n}{2}u_i^n, \quad 1 < i < M; \quad m_0^n = \frac{x_1^n - x_0^n}{2}u_0^n; \quad \text{and} \quad m_M^n = \frac{x_M^n - x_{M-1}^n}{2}u_M^n. \quad (3.17)$$

It follows from (3.14)-(3.15) that

$$m_i^n \equiv m_i^0, \quad 0 \leq i \leq M, \quad n = 1, 2, \dots, N.$$

Since $x^n \in \mathcal{Q}$, we know that $u_i^n > 0$, $0 \leq i \leq M$, $n = 1, 2, \dots, N$. □

3.3 Numerical Scheme for Problems with Free Boundaries

For the initial data with a compact support in Ω , we define the left and right interfaces as

$$\xi_1^t := \inf\{x \in \Omega : u(x, t) > 0, t \geq 0\}, \quad (3.18)$$

$$\xi_2^t := \sup\{x \in \Omega : u(x, t) > 0, t \geq 0\}. \quad (3.19)$$

Let $\Gamma^t := [\xi_1^t, \xi_2^t] \subset \Omega$. Assume $H(\cdot) \in C^2([0, +\infty))$ and $f(\cdot) \in C^1([0, +\infty))$ with $f'(0) \neq 0$.

We shall solve the initial-boundary value problem (2.9) with the boundary condition

$$x_t = -f'(0) \frac{\partial_X u_0(X)}{(\partial_X x)^2} H'' \left(\frac{u_0(X)}{\partial_X x} \right) - f'(0)V'(x) - f'(0)\mathcal{S}(x), \quad X \in \partial\Gamma^0, \quad (3.20)$$

and the initial condition

$$x(X, 0) = X, \quad X \in \Gamma^0, \quad (3.21)$$

where time $t > 0$ and $\mathcal{S}(x)$ is given by (2.7). Here the boundary condition (3.20) on the free boundary is obtained from (2.9) with the condition $u_0(X)|_{\partial\Gamma} = 0$.

We partition the interval Γ^0 into equal subintervals with $X_i = \xi_1^0 + ih$, $0 \leq i \leq M$, where M is an integer number and the grid spacing $h := (\xi_2^0 - \xi_1^0)/M$. Given the initial state $u_0(X)$ with a compact support Γ^0 , the numerical solution for the trajectory equation is obtained by solving (3.8) for $1 \leq i \leq M - 1$, and discrete boundary conditions

$$\begin{aligned} \frac{x_i^{n+1} - x_i^n}{\tau} = & -f'(0) \cdot H'' \left(\frac{u_0(X)}{\tilde{D}_h x_i^{n+1}} \right) \cdot \frac{\tilde{D}_h u_0(X)}{(\tilde{D}_h x_i^{n+1})^2} - f'(0) V_c'(x_i^{n+1}) \\ & + f'(0) V_e'(x_i^n) - f'(0) \hat{\mathcal{S}}_{c_i}^{n+1} + f'(0) \hat{\mathcal{S}}_{e_i}^n \quad \text{for } i = 0 \text{ and } M, \end{aligned} \quad (3.22)$$

where $\hat{\mathcal{S}}_{c_i}^{n+1}$ and $\hat{\mathcal{S}}_{e_i}^n$ are given by (3.10) and (3.11), respectively. The whole nonlinear system is again solved by a Newton's iteration method.

The waiting time phenomenon, i.e., a free boundary remains stationary during $(0, t^*)$ for $0 < t^* < \infty$, may occur under some conditions. Such a phenomenon is common and important for the porous medium type of equations [50, 2]. However, the development of efficient algorithms for the calculation of waiting time is challenging. Based on the Energetic Variational Approach, we have proposed an algorithm to calculate the waiting time for porous medium equations in [24]. In this work, we extend the algorithm to consider more general problems described by the nonlinear Fokker–Planck equations that have the waiting time phenomenon.

As the right hand side of the equation (3.20) vanishes, the free boundaries remain stationary. Without loss of generality, we consider the left boundary. Analogous results can be obtained for the right boundary. The waiting time can be characterized by

$$t^* := \inf \left\{ t > 0 : x_t < 0, \text{ as } X \rightarrow \xi_1^0 \right\}.$$

We define

$$\begin{aligned} \mathcal{B}_h^n := & f'(0) H'' \left(\frac{u_0(X)}{\tilde{D}_h x_{h,0}^n} \right) \cdot \frac{\tilde{D}_h u_0(X)}{(\tilde{D}_h x_{h,0}^n)^2} + f'(0) V_c'(x_{h,0}^n) \\ & - f'(0) V_e'(x_{h,0}^n) + f'(0) \hat{\mathcal{S}}_{c_0}^{n+1} - f'(0) \hat{\mathcal{S}}_{e_0}^n, \end{aligned}$$

where $x_h^n = (x_{h,0}^n, \dots, x_{h,M}^n)$ denotes the numerical solution at time t^n , $n = 0, \dots, N$, with a grid spacing h . The waiting time t_h^* is numerically determined by the criterion [24]

$$t_h^* := \min \left\{ t^n : \left| \frac{\mathcal{B}_{2h}^n}{\mathcal{B}_h^n} \right| \leq 1 \right\}. \quad (3.23)$$

4 Analysis Results

In this section, we perform numerical analysis on the numerical scheme (3.8), including unique solvability in the admissible set, total energy dissipation, and convergence rate.

Theorem 4.1. *Assume that $H(\cdot)$, $V_c(\cdot)$, $V_e(\cdot)$, $W_c(\cdot)$, and $W_e(\cdot)$ are piecewise C^1 functions. If the initial state $u_0(X) \in \mathcal{E}_M$ is positive for $X \in \mathcal{Q}$, then the numerical scheme (3.8) is uniquely solvable in \mathcal{Q} .*

Proof: We first consider the following optimization problem

$$\min_{z \in \bar{\mathcal{Q}}} J(z),$$

where the functional J is given in (3.12). Since $J(z)$ is a convex functional on the closed convex set $\bar{\mathcal{Q}}$, there exists a unique minimizer $x \in \bar{\mathcal{Q}}$. For any $z \in \partial\mathcal{Q}$, there exists some $i > 0$ such that $(D_h z)_{i-1/2} = (z_i - z_{i-1})/h = 0$, indicating that $J(z) = +\infty$. Therefore, we have that the minimizer $x \in \mathcal{Q}$. Next we shall prove that x is the minimizer of $J(z)$ if and only if it solves the equations (3.8). We then claim that the fully discrete scheme (3.8) has a unique solution.

Suppose $x \in \mathcal{Q}$ is the minimizer of $J(z)$. Since \mathcal{Q} is an open convex set, for any $z \in \bar{\mathcal{Q}}$, there exists a sufficiently small $\varrho_0 > 0$, such that, for $\varrho \in (-\varrho_0, \varrho_0)$, $x + \varrho(z - x) \in \mathcal{Q}$. Then $j(\varrho) := J(x + \varrho(z - x))$ achieves its minimum at $\varrho = 0$. So we have $j'(0) = 0$. By the summation by parts (3.7), we obtain for any $z \in \bar{\mathcal{Q}}$ that

$$\begin{aligned} & \frac{1}{\tau} \left\langle \frac{u_0^2}{\bar{D}_h x^n} \cdot \frac{1}{f\left(\frac{u_0(X)}{\bar{D}_h x^n}\right)} \cdot (x - x^n), z - x \right\rangle_{\mathcal{E}} + \left\langle d_h \left(\frac{u_0}{D_h x} H' - H \right), z - x \right\rangle_{\mathcal{E}} \\ & + \langle u_0(X) V'_c(x), z - x \rangle_{\mathcal{E}} + \langle u_0(X) \langle W'_c(x - y), u_0(Y) \rangle, z - x \rangle_{\mathcal{E}} \\ & - \langle u_0(X) V'_e(x^n), z - x \rangle_{\mathcal{E}} - \langle u_0(X) \langle W'_e(x^n - y^n), u_0(Y) \rangle, z - x \rangle_{\mathcal{E}} = 0. \end{aligned} \quad (4.1)$$

This implies that x solves the equations (3.8).

Conversely, let x be a solution to the fully discrete scheme (3.8). We shall prove that x is the minimizer of $J(z)$ on $\bar{\mathcal{Q}}$. For any $z \in \partial\mathcal{Q}$, we have $J(z) \geq J(x)$ due to $J(z) = +\infty$. For any $z \in \mathcal{Q}$, taking an inner product of (3.8) with $z - x$ and using summation by parts lead to (4.1). By the convexity of $J(z)$ and (4.1), we have for any $z \in \mathcal{Q}$ that

$$J(z) = J(x + (z - x)) \geq J(x). \quad (4.2)$$

This completes the proof. \square

We next consider discrete energy dissipation of the numerical scheme (3.8). The discrete total energy $E_N : \mathcal{Q} \rightarrow \mathbb{R}$ corresponding to (3.1) is defined by

$$E_N(x) := \left\langle H \left(\frac{u_0(X)}{D_h x} \right), D_h x \right\rangle_c + \langle u_0(X), V(x) \rangle_{\mathcal{E}} + \frac{1}{2} \langle u_0(X), \langle W(x - y), u_0(Y) \rangle \rangle_{\mathcal{E}}. \quad (4.3)$$

Analogously, we have the splitting $E_N(x) = E_{N,c}(x) - E_{N,e}(x)$, where

$$E_{N,c}(x) := \left\langle H \left(\frac{u_0(X)}{D_h x} \right), D_h x \right\rangle_c + \langle u_0(X), V_c(x) \rangle_{\mathcal{E}} + \frac{1}{2} \langle u_0(X), \langle W_c(x - y), u_0(Y) \rangle \rangle_{\mathcal{E}},$$

$$E_{N,e}(x) := \langle u_0(X), V_e(x) \rangle_{\mathcal{E}} + \frac{1}{2} \langle u_0(X), \langle W_e(x - y), u_0(Y) \rangle \rangle_{\mathcal{E}}.$$

Here both $E_{N,c}(x)$ and $E_{N,e}(x)$ are convex and their first variations are given by

$$\delta_x E_{N,c}(x^{n+1}) = d_h \left[\frac{u_0(X)}{D_h x^{n+1}} \cdot H' \left(\frac{u_0(X)}{D_h x^{n+1}} \right) - H \left(\frac{u_0(X)}{D_h x^{n+1}} \right) \right] + u_0(X) V'_c(x^{n+1}) + \mathcal{S}_{N_c}^{n+1}, \quad (4.4)$$

$$\delta_x E_{N,e}(x^n) = u_0(X) V'_e(x^n) + \mathcal{S}_{N_e}^n. \quad (4.5)$$

Theorem 4.2. Suppose $x^n = (x_0^n, \dots, x_M^n) \in \mathcal{Q}$ be the solution to the scheme (3.8) at time t^n . Denote by $E_N^n := E_N(x^n)$. Then the discrete energy dissipation law holds, i.e.,

$$\frac{E_N^{n+1} - E_N^n}{\tau} \leq - \left\langle \frac{u_0^2(X)}{\tilde{D}_h x^n} \cdot \frac{1}{f\left(\frac{u_0(X)}{\tilde{D}_h x^n}\right)} \cdot \frac{x^{n+1} - x^n}{\tau}, \frac{x^{n+1} - x^n}{\tau} \right\rangle_{\mathcal{E}} \leq 0, \quad n = 0, 1, \dots \quad (4.6)$$

This is the discrete counterpart of the dissipation law (2.3).

It is easy to prove the theorem by using the convexity of $E_{N,c}^n$ and $E_{N,e}^n$. Similar ideas can be found in the works [23, 24, 25].

Theorem 4.3. Assume that there exist positive constants b_{u_0} and B_{u_0} , such that the initial condition $u_0(X)$ satisfies $b_{u_0} \leq u_0(X) \leq B_{u_0}$. Assume that $f(\cdot)$ and $H(\cdot) \in C^2([0, \infty))$, and $V_c(\cdot)$, $V_e(\cdot)$, $W_c(\cdot)$, and $W_e(\cdot) \in C^2(\bar{\Omega})$. Denote by $x_e \in \Omega$ the exact solution to the trajectory equation (2.9) with sufficient regularity and $x_h \in \mathcal{Q}$ the numerical solution to the numerical scheme (3.8). The numerical error function is defined by

$$e_i^n = x_{e_i}^n - x_i^n, \quad (4.7)$$

where $x_e^n, x^n \in \mathcal{Q}$, $0 \leq i \leq M$, $n = 0, \dots, N$. Then

- $e^n = (e_0^n, \dots, e_M^n)$ satisfies

$$\|e^n\| := \langle e^n, e^n \rangle_{\mathcal{E}} \leq C(\tau + h^2).$$

- $\tilde{D}_h e^n = (\tilde{D}_h e_0^n, \dots, \tilde{D}_h e_M^n)$ satisfies

$$\|\tilde{D}_h e^n\| \leq C(\tau + h^2).$$

Moreover, numerical error between the numerical solution u_h^n and exact solution u_e^n to the problem (1.1) is estimated by

$$\|u_h^n - u_e^n\| \leq C(\tau + h^2), \quad n = 0, \dots, N,$$

where C is a positive constant, h is the grid spacing, and τ is the time step size.

The theorem can be proved by using a careful high-order asymptotic expansion and two-step error estimates, as shown in the work [25]. The details of the proof are quite involved and will be presented in our future work.

The following theorem presents that our numerical method also preserves steady states.

Theorem 4.4. (Steady-state preserving) Assume $u_0(x) > 0$ and the discrete energy E_N^n is bounded below. The fully discrete scheme (3.8) and (3.9) is steady-state preserving in the sense that, for fixed h , as the time step $n \rightarrow \infty$, the numerical solution $\{x_i^\infty\}_{i=0}^M \in \mathcal{Q}$ is a numerical solution to a boundary-value problem (BVP) for steady states:

$$\begin{cases} -\partial_X \left[\frac{u_0(X)}{\partial_X x^\infty} H' \left(\frac{u_0(X)}{\partial_X x^\infty} \right) - H \left(\frac{u_0(X)}{\partial_X x^\infty} \right) \right] - u_0(X) V'(x^\infty) \\ \quad - u_0(X) \int_{\Omega} W'(x^\infty(X, t) - y^\infty(Y, t)) u_0(Y) dY = 0, \\ x^\infty|_{\partial\Omega} = X|_{\partial\Omega}. \end{cases} \quad (4.8)$$

Proof: The energy dissipation in Lagrangian coordinate reads

$$\frac{d}{dt}E^{total} = -\Delta, \quad (4.9)$$

where the entropy production

$$\begin{aligned} \Delta = \int_{\Omega} f\left(\frac{u_0(X)}{\partial_X x}\right) \cdot \frac{\partial_X x}{u_0^2(X)} \left| \partial_X \left[\frac{u_0(X)}{\partial_X x} H'\left(\frac{u_0(X)}{\partial_X x}\right) - H\left(\frac{u_0(X)}{\partial_X x}\right) \right] \right. \\ \left. + u_0(X)V'(x) + u_0(X) \int_{\Omega} W'(x(X,t) - y(Y,t))u_0(Y)dY \right|^2 dX. \end{aligned}$$

The energy dissipation (4.9) implies that steady states are achieved when the trajectory x^∞ satisfies the BVP (4.8).

Since the discrete total energy E_N^n decreases monotonically and is bounded below, the limit $E_N^\infty := \lim_{n \rightarrow \infty} E_N^n$ exists. By the discrete energy dissipation law (4.6), we have

$$\lim_{n \rightarrow \infty} \left\langle \frac{u_0^2(X)}{\widetilde{D}_h x^n} \cdot \frac{1}{f\left(\frac{u_0(X)}{\widetilde{D}_h x^n}\right)} \cdot \frac{x^{n+1} - x^n}{\tau}, \frac{x^{n+1} - x^n}{\tau} \right\rangle_{\mathcal{E}} = 0, \quad x^{n+1}, x^n \in \mathcal{Q}.$$

This along with the fully discrete scheme (3.8) deduces that the numerical solution $\{x_i^\infty\}_{i=0}^M$ solves the difference equations

$$\begin{cases} -d_h \left[\frac{u_0}{D_h x^\infty} \cdot H'\left(\frac{u_0}{D_h x^\infty}\right) - H\left(\frac{u_0}{D_h x^\infty}\right) \right]_i - u_{0_i} V(x_i^\infty) \\ \quad - u_{0_i} \langle W'(x_i^\infty - y^\infty), u_0(Y) \rangle_{\mathcal{E}} = 0, \quad i = 1, \dots, M-1, \\ x_0^\infty = X_0 \text{ and } x_M^\infty = X_M, \end{cases} \quad (4.10)$$

which are exactly a second-order finite difference discretization to the BVP (4.8). Thus, $\{x_i^\infty\}_{i=0}^M$ is a numerical solution to the BVP (4.8). \square

5 Numerical Results

In this section, we present numerical examples to demonstrate advantages of our numerical methods in solving the Fokker-Planck equation with nonlinear diffusion, various nonlocal interaction kernels, and free boundaries with waiting time phenomena. In the following numerical simulations, we first solve the trajectory equation (2.9) with the initial and boundary conditions (3.20)-(3.21) using the fully discrete scheme (3.8) with (3.22), and then approximate the density function u in (2.5) by (3.14)-(3.15).

We define the error of numerical solutions e_h in \mathcal{L}^2 , \mathcal{L}^1 , and \mathcal{L}^∞ norms as follows

$$\|e_h\|_2^2 := \left(\frac{1}{2}e_{h_0}^2 h_{x_0} + \sum_{i=1}^{M-1} e_{h_i}^2 h_{x_i} + \frac{1}{2}e_{h_M}^2 h_{x_M} \right), \quad (5.1)$$

$$\|e_h\|_1 = \left(\frac{1}{2}|e_{h_0}|h_{x_0} + \sum_{i=1}^{M-1} |e_{h_i}|h_{x_i} + \frac{1}{2}|e_{h_M}|h_{x_M} \right), \quad (5.2)$$

and

$$\|e_h\|_\infty = \max_{0 \leq i \leq M} \{|e_{h_i}|\}, \quad (5.3)$$

where $e_h = (e_{h_0}, e_{h_1}, \dots, e_{h_M})$. Note that the error of the numerical trajectory $e_h^x := x_e - x$ is given on the mesh with

$$h_{x_i} = h, \quad 0 \leq i \leq M,$$

where x_e is the exact solution of the trajectory on the grid and h is a uniform grid spacing; and the error of the density $e_h^u := u_e - u$ is given on the mesh with

$$h_{x_i} = \frac{x_{i+1} - x_{i-1}}{2}, \quad 1 \leq i \leq M-1, \quad h_{x_0} = x_1 - x_0, \quad h_{x_M} = x_M - x_{M-1},$$

where u_e is the exact solution of density on the grid.

5.1 Porous Medium Type of Equations

In this section, we focus on the porous medium type of equations with one-well and double-well potentials, which have waiting time phenomena.

Example 1: Porous medium equation with one-well potential

We consider the following nonlinear equation

$$\partial_t u = \partial_x \left[u \partial_x \left(\frac{m}{m-1} u^{m-1} + \frac{x^2}{2} \right) \right], \quad x \in [-2, 2], \quad (5.4)$$

which corresponds to the FP equations with $f(u) = u$, $H(u) = \frac{1}{m-1} u^m$, $V(x) = \frac{x^2}{2}$, and $W = 0$. This equation has been studied in [13, 48]. This equation with zero-flux boundary conditions has a steady state

$$u_\infty(x) = \left(C - \frac{m-1}{2m} |x|^2 \right)^{\frac{1}{m-1}},$$

where the constant C is determined by ensuring the mass conservation. Moreover, the relative total energy $E(t|\infty) = E(u(t)) - E(u_\infty)$ decays exponentially, i.e., $E(t|\infty) \leq E(0|\infty)e^{-2t}$. Here the decay rate e^{-2t} is sharp.

Let $m = 2$. We take the same compact supported initial data as in [48]:

$$u(x, 0) = \max\{1 - |x|, 0\}, \quad x \in [-2, 2]. \quad (5.5)$$

The corresponding stationary solution is given in [13, 48]:

$$u_\infty = \max \left\{ \left(\frac{3}{8} \right)^{\frac{2}{3}} - \frac{x^2}{4}, 0 \right\}. \quad (5.6)$$

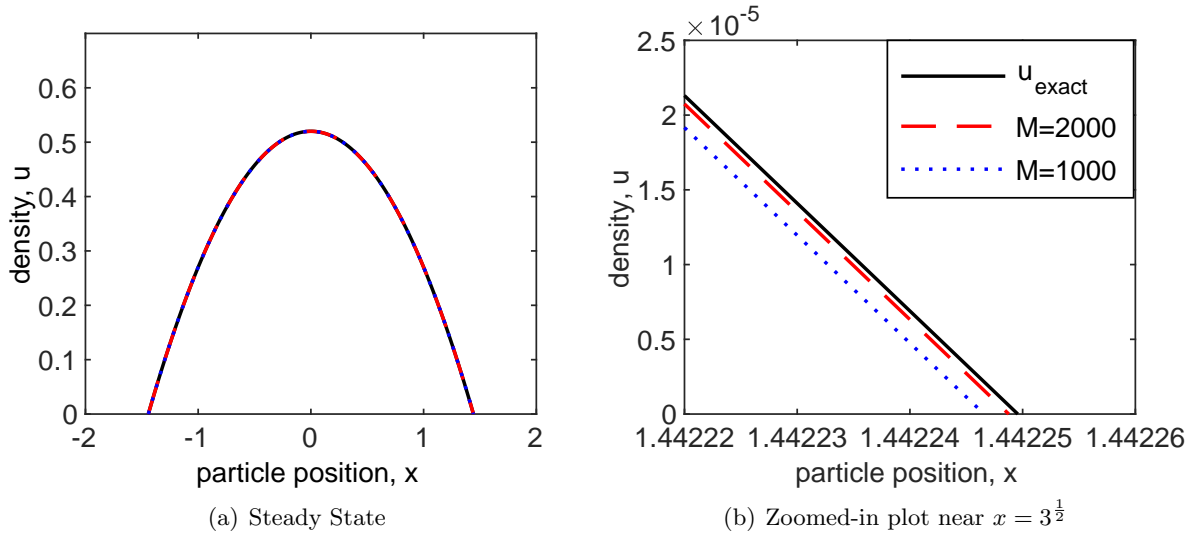


Figure 1: Numerical solution and the exact solution of the steady-state density of **Example 1** with $\tau = 1/2000$ and $m = 2$.

We numerically simulate the problem on meshes with $M = 1000$ and $M = 2000$ up to time $T = 10$, at which the problem can be identified as the steady state. Fig. 1 (a) shows the numerical solution and exact solution (5.6) at the steady state. Clearly, one can observe that the numerical solution can approximate the exact solution accurately. To have detailed comparison, we display a zoomed-in plot near the free boundary $x = 3^{\frac{1}{2}}$ in Fig. 1 (b). As the mesh refines, the numerical solution can effectively approach the exact solution near the free boundary *without any oscillation*.

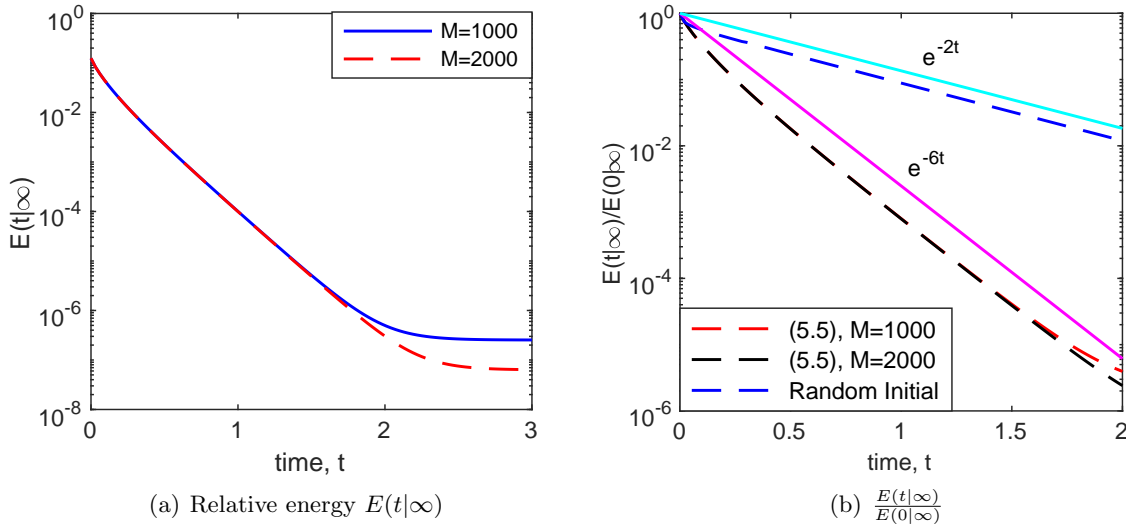


Figure 2: The evolution of the relative energy of the equation (5.4) with the initial condition (5.5) and a random initial condition in **Example 1** ($\tau = h/2$ and $m = 2$).

Furthermore, we show in Fig. 2 (a) the relative total energy. One can see that the relative total energy decays monotonically and remains positive as time evolves for both $M = 1000$ and $M = 2000$. To further check the decay rate, we present the relative total energy rescaled by its initial value in Fig. 2 (b), which displays that the decay rate is around e^{-6t} for the equation (5.4) with the initial condition (5.5). To investigate more on the decay rate, we also study the equation (5.4) with a random initial condition. The dashed blue curve shown in Fig. 2 (b) demonstrates that $\frac{E(t|\infty)}{E(0|\infty)} \leq e^{-2t}$, being consistent with the theoretical result [13].

| h | τ | $\ e_h^u\ _2$ | Order | $\ e_h^u\ _1$ | Order | $\ e_h^u\ _\infty$ | Order |
|-------|--------|---------------|-------|---------------|-------|--------------------|-------|
| 1/50 | 1/100 | 1.015e-03 | | 2.894e-04 | | 5.193e-03 | |
| 1/100 | 1/400 | 3.597e-04 | 1.497 | 7.292e-05 | 1.989 | 2.598e-03 | 0.999 |
| 1/200 | 1/1600 | 1.273e-04 | 1.498 | 1.830e-05 | 1.994 | 1.300e-03 | 0.999 |
| 1/400 | 1/6400 | 4.505e-05 | 1.499 | 4.584e-06 | 1.997 | 6.499e-04 | 1.000 |

Table 1: Numerical error and convergence order of the numerical solution at time $T = 10$ for **Example 1**.

We further consider the numerical accuracy of our numerical method with various mesh resolution. Table 1 shows that the numerical error and convergence rate for the solution u at time $T = 10$ in the \mathcal{L}^1 , \mathcal{L}^2 and \mathcal{L}^∞ norms. We observe that our numerical method has convergence order of 2 in the \mathcal{L}^1 norm, $\frac{3}{2}$ in the \mathcal{L}^2 norm, and 1 in the \mathcal{L}^∞ norm. It is believed that the low regularity near the free boundary accounts for the decrease of convergence order. We remark that, to the best of our knowledge, the convergence order of numerical schemes for the Fokker-Planck equations with the presence of free boundaries has not been studied in the literature.

Example 2: Porous medium equation with a double-well potential

In this example, we consider the degenerate Fokker-Planck equations with a double-well potential:

$$\partial_t u = \partial_x \{ u \partial_x [\nu u^{m-1} + V(x)] \}, \quad x \in [-2, 2], \quad (5.7)$$

in which $f(u) = u$, $H'(u) = \nu u^{m-1}$, $V(x) = x^4/4 - x^2/2$, and $W = 0$. The steady state is given by

$$u_\infty = \left(\frac{c(x) - V(x)}{\nu} \right)_+^{1/(m-1)}, \quad (5.8)$$

where $c(x)$ is a piecewise constant [17, 35, 42].

To demonstrate the accuracy of our numerical schemes, we solve the problem (5.7) with a positive initial condition

$$u_0 = \frac{M}{\sqrt{2\pi\sigma^2}} e^{-\frac{x^2}{2\sigma^2}}, \quad x \in [-2, 2], \quad (5.9)$$

where $M = 4.2517 \times 10^{-2}$ and $\sigma = \sqrt{0.2}$. Then $c(x) = -\frac{3}{16}$ in (5.8).

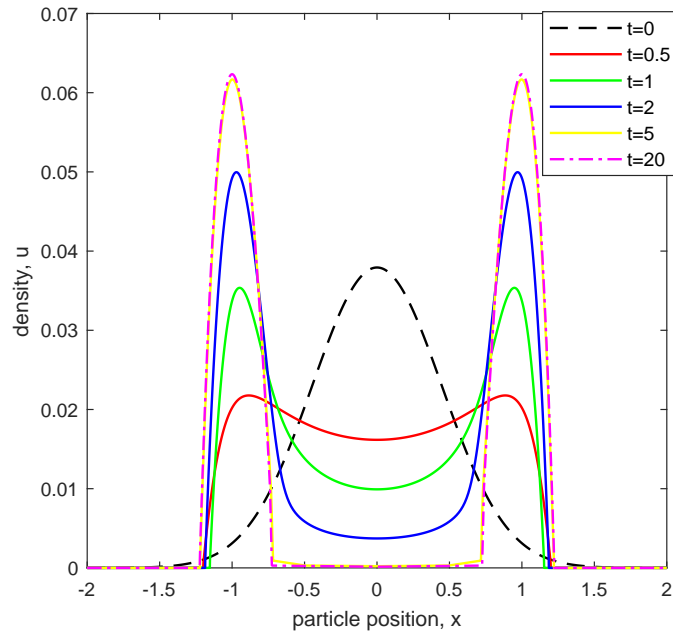


Figure 3: The evolution of the numerical density in **Example 2** with $h = 1/1000$, $\tau = 1/1000$, and $m = 2$.

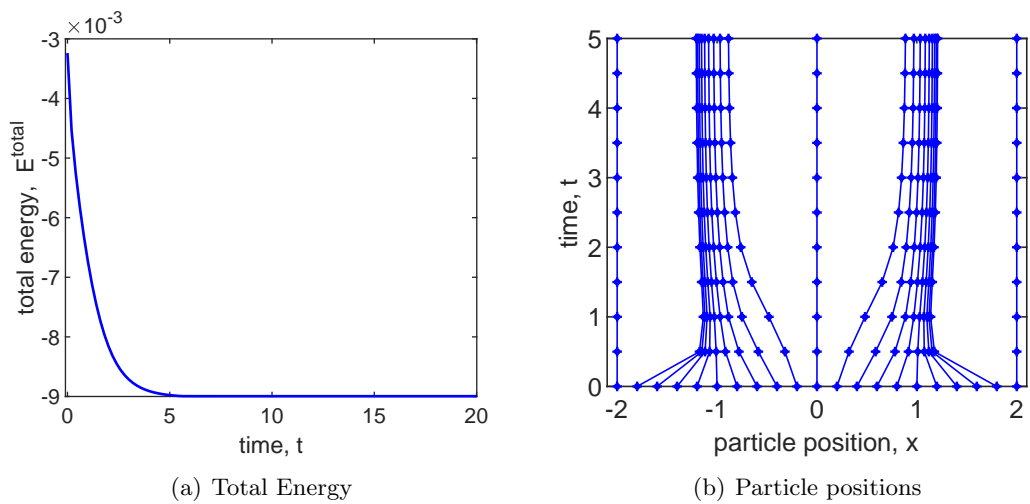


Figure 4: The evolution of the total energy and particle positions in **Example 2** with $h = 1/1000$, $\tau = 1/1000$, and $m = 2$.

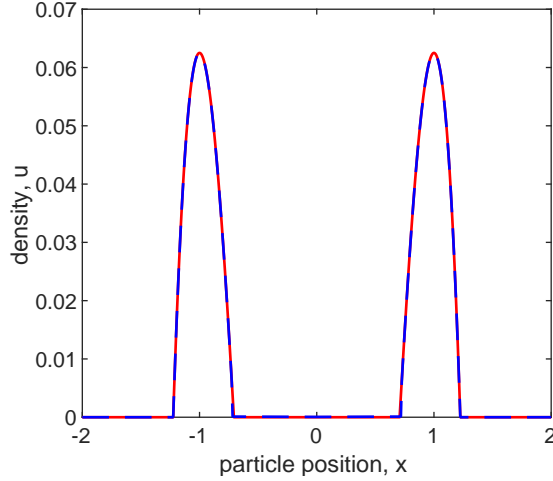


Figure 5: The numerical solution u_h (the blue line) and exact solution u_e (the red dotted line) at the steady state ($T = 20$) in **Example 2** with $h = 1/1000$, $\tau = 1/1000$, and $m = 2$.

Fig. 3 shows the evolution of density u with $h = 1/1000$, $\tau = 1/1000$, and $m = 2$ up to time $T = 20$. Due to the external double-well potential, the solution gradually splits into two parts, localizing at the two centers of the wells. Long-time simulation up to the time $T = 20$ shows the asymptotic convergence of the numerical solution towards a steady state. Fig. 4 (a) and (b) show the decay of the total energy and motion of particles that move towards the two centers with a finite speed. Fig. 5 shows that the numerical solution and exact solution at the steady state are almost identical.

| h | τ | $\ e_h^u\ _2$ | Order | $\ e_h^u\ _\infty$ | Order |
|-------|---------|---------------|-------|--------------------|-------|
| 0.02 | 0.02 | 5.606e-05 | | 5.962e-05 | |
| 0.01 | 0.005 | 1.422e-05 | 1.979 | 1.509e-05 | 1.983 |
| 0.005 | 0.00125 | 4.170e-06 | 1.769 | 3.781e-06 | 1.996 |
| h | τ | $\ e_h^x\ _2$ | Order | $\ e_h^x\ _\infty$ | Order |
| 0.02 | 0.02 | 1.619e-02 | | 2.390e-02 | |
| 0.01 | 0.005 | 4.334e-03 | 1.979 | 6.485e-03 | 1.882 |
| 0.005 | 0.00125 | 1.106e-03 | 1.770 | 1.694e-03 | 1.936 |

Table 2: Numerical error and convergence order of the numerical trajectory x and density u at time $T = 0.1$ in **Example 2**.

| h | τ | $\ e_h^u\ _2$ | Order | $\ e_h^u\ _\infty$ | Order |
|-------|--------|---------------|--------|--------------------|--------|
| 1/50 | 1/50 | 1.3554e-02 | | 1.5146e-02 | |
| 1/100 | 1/200 | 9.7065e-03 | 0.4817 | 1.1056e-02 | 0.4541 |
| 1/200 | 1/800 | 6.9297e-03 | 0.4862 | 7.9973e-03 | 0.4673 |
| 1/400 | 1/3200 | 4.9353e-03 | 0.4897 | 5.7471e-03 | 0.4767 |

Table 3: Numerical error and convergence order of the numerical density u at the steady state in **Example 2**.

Table 2 presents the numerical error and convergence order of both the numerical trajectory x and density u at time $T = 0.1$. Note that the reference exact solution is obtained numerically on a rather refined mesh with $h = 10^{-5}$ and $\tau = 10^{-6}$. One observes that the numerical method is roughly second order accurate in space and first order accurate in time at time $T = 0.1$. However, the numerical convergence order degenerates to 0.5 in space at the steady state in Table 3, due to the lower regularity of the solution close to the free boundaries; cf. the solution profile with a support in Fig. 3.

Example 3: Waiting time phenomena with nonlocal interactions

In this example, we consider a nonlinear diffusion system with the waiting time phenomena, which are commonly found in the porous medium type of diffusion [2, 50, 24]. The challenge lies in establishing an efficient algorithm for the calculation of waiting time. One related algorithm has been proposed in the work [24] to compute the waiting time for the porous medium equation. We now extend the algorithm to solve a more complex problem (1.1) with $f(u) = u$, $H(u) = \frac{\nu}{m}u^m$, $V(x) = -\frac{(x+\frac{\pi}{2})^2}{2}$, $W(x) = \frac{4-\theta}{8}|x|$, and the initial condition

$$u_0(x) = \left\{ \frac{m-1}{m} [(1-\theta)\sin^2(x) + \theta\sin^4(x)] \right\}^{1/(m-1)}, \quad x \in [-\pi, 0],$$

where $\theta \in [0, 1]$ is a parameter. Note that the nonlocal interaction kernel $W(x)$ here is not differentiable at $x = 0$. To address this issue, we split the integral (2.7) into two integrals on two domains with the non-differentiable location as the integration upper and lower limits of such two integrals. In each integral, the $W'(0)$ is understood as $W'(0\pm)$. We employ a mesh with a total spatial grid number $M = 100$ and a time step size $\tau = 1/100$. Let $m = 2$ and $\nu = 2$.

Fig. 6 shows evolution of the profile of the density u with $m = 2$ from $t = 0$ to $t = 1$. The estimated waiting time is about $t^* = 0.31$. During the time evolution, the numerical solution is free of oscillation near free boundaries and the boundaries have finite-speed propagation after exceeding the waiting time. Fig. 7 (a) shows trajectories of particles as time evolves. One can find that the boundaries remain stationary up to time $t^* = 0.31$, as indicated by the red dash line, and then move outward at a finite speed. Fig. 7 (b) displays the relationship between the waiting time t^* and θ . We can see that the waiting time t^* increases monotonically as θ grows.

5.2 Nonlinear Fokker–Planck Equations

Example 4: Generalized Fokker–Planck Equations for Boson Gas

In this example, we focus on the generalized Fokker–Planck equation with a superlinear drift:

$$\partial_t u = \partial_x [xu(1 + u^K) + \partial_x u], \quad (5.10)$$

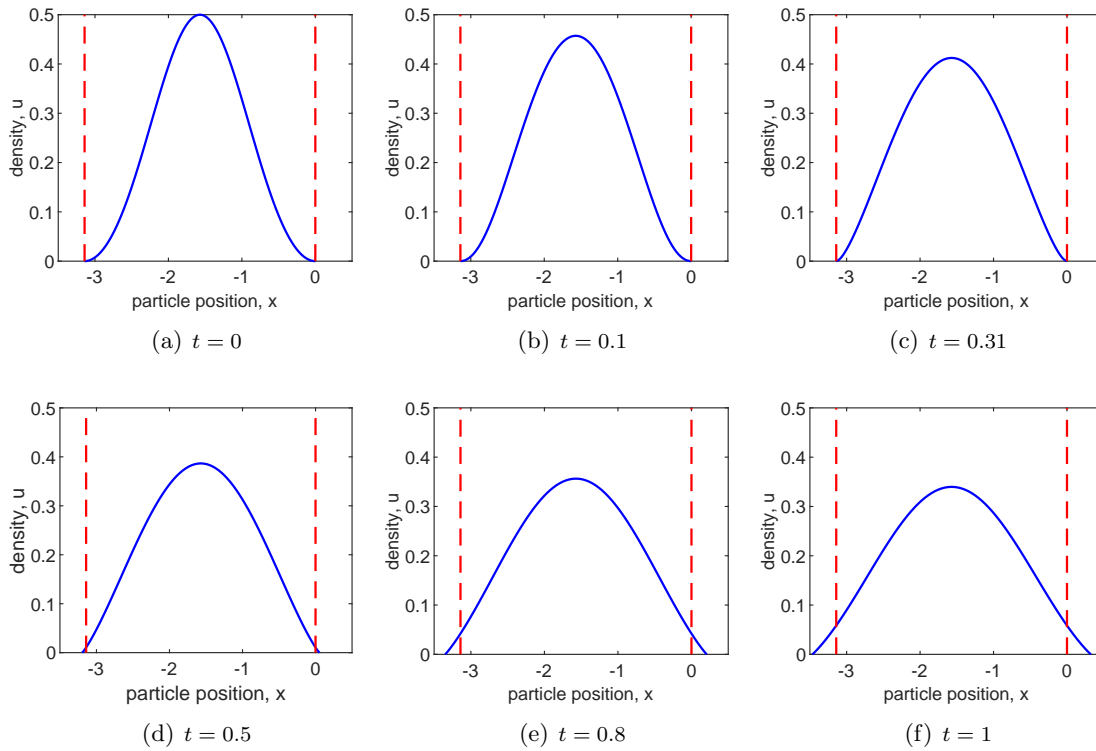


Figure 6: Evolution of the profile of the density u from $t = 0$ to $t = 1$ with $\theta = 0.25$ in **Example 3**.

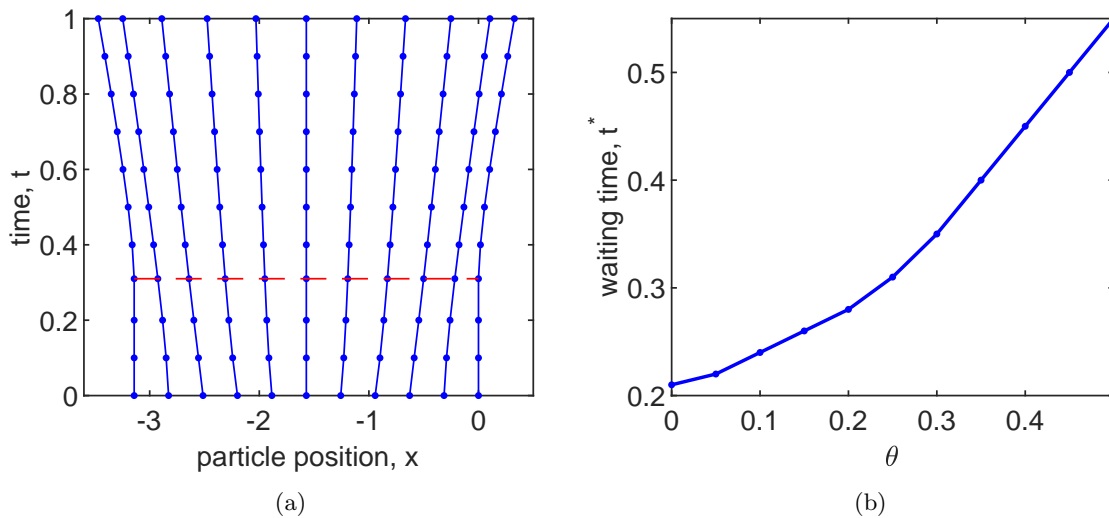


Figure 7: (a) Evolution of particles with $\theta = 0.25$; (b) The relationship between θ and the waiting time t^* in **Example 3**.

where K is a positive constant. For $K > 2$, the system exhibits a critical mass phenomenon [1], i.e., an initial distribution with supercritical mass leads to singularity at the origin. The phenomenon has been confirmed numerically in [7, 35, 48], in which the numerical solution approximates singularity with precision dependent on mesh resolution, i.e., $\mathcal{O}(1/h)$ with h being the grid spacing. In this work, we shall show that the approximation precision of singularity can be enhanced significantly by our numerical methods.

We take $f(u) = u(1 + u^3)$, $H'(u) = \log(\frac{u}{\sqrt[3]{1+u^3}})$, $V(x) = \frac{\beta}{2}x^2$, and $W = 0$ in (1.1). The initial data is given by

$$u_0(x) = \frac{M}{2\sqrt{2\pi}} \left(e^{-\frac{(x-2)^2}{2}} + e^{-\frac{(x+2)^2}{2}} \right), \quad x \in [-6, 6].$$

Thus the trajectory equation becomes

$$\partial_t x = - \left[1 + \left(\frac{u_0(X)}{\partial_X x} \right)^3 \right] \cdot \left[\frac{1}{\partial_X x} \log \left(\frac{u_0(X)/\partial_X x}{\sqrt[3]{1 + (u_0(X)/\partial_X x)^3}} \right) + \beta x \right]. \quad (5.11)$$

Remark 5.1. *When the distances between particles get less than machine precision, they are indistinguishable in numerical calculations and the numerical solution may blow up. To avoid losing accuracy of density u in (3.14), we merge those particles together in our numerical treatment and regard them as one particle with the density changed accordingly. As a rule of thumb, we choose a criterion with a tolerance $\varepsilon_0 = 10^{-9}$ and define*

$$\mathcal{R} := \{x_i^{n+1} | x_{i+1}^{n+1} - x_i^{n+1} \leq \varepsilon_0, i = 0, \dots, M-1\}. \quad (5.12)$$

If $\mathcal{R} \neq \emptyset$, there must be some particles that have been merged together at time t^{n+1} . See the work [23] for more details on the numerical implementation.

We first consider $\beta = 1$. Fig. 9 and 10 present the density u for the cases with subcritical mass $M = 1$ and supercritical mass $M = 10$, respectively. One can see that the solution remains bounded with subcritical mass, and the solution blows up at a finite time with supercritical mass, being consistent with the theoretical conclusion made in [1] and the numerical observation in [7, 35, 48]. One remarkable advantage of our numerical method is that the numerical solution obtained by the scheme (3.8) approximates the singularity of the scale $\mathcal{O}(1/\varepsilon_0)$, with the small positive ε_0 close to the machine precision. Fig. 8 (a) displays that the entropy decays monotonically and remains positive as time evolves for the subcritical case. Fig. 8 (b) shows the concentration process of particles towards the origin for $M = 1$. Fig. 11 (a) and (b) show the evolution of entropy and total mass for the case with supercritical mass $M = 10$. We can see that the entropy decays exponentially to zero and the total mass remains constant. Fig. 12 (a) shows the evolution of mass at the central point for the case with supercritical mass $M = 10$ and $\beta = 1$. The increase of mass reveals that the particles accumulate at the central point. A saturation mass, related to the value of ε_0 , is achieved when the concentration process balances the diffusion process. Also, we study the relationship between β and the critical mass in Fig. 12 (b). As β grows, the force exerted by the external potential $V(x)$ gets stronger and the critical mass decreases correspondingly.

5.3 Aggregation-diffusion Models

We now consider the Fokker–Planck equations with nonlocal interaction kernels. The Fokker–Planck equations with a smooth kernel have been studied in [10], which has proved that, under

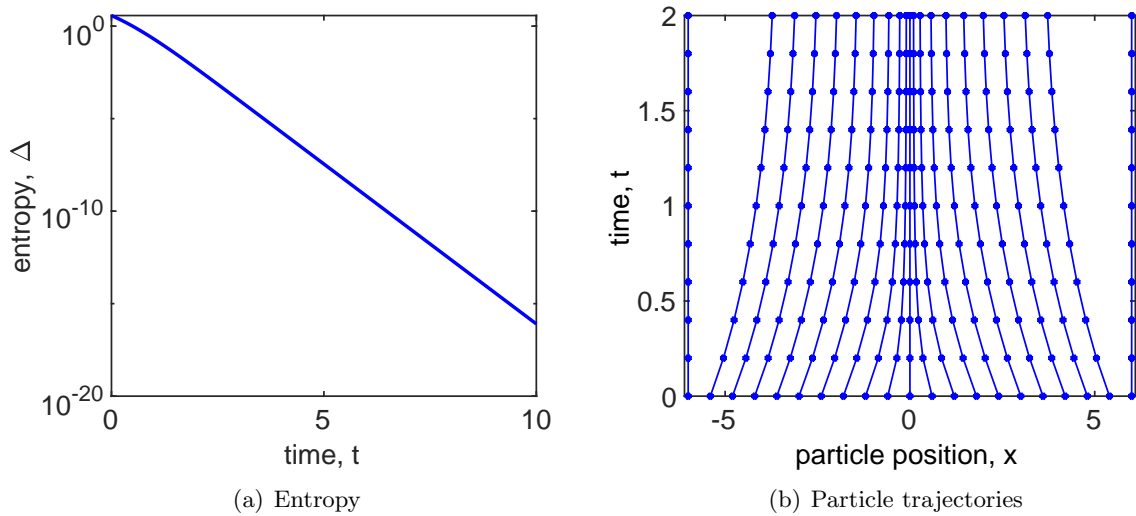


Figure 8: The evolution of entropy and particle trajectories for the case with subcritical mass $M = 1$ and $\beta = 1$ in **Example 4** ($h = 1/1000$, $\tau = 1/1000$, $m = 2$).

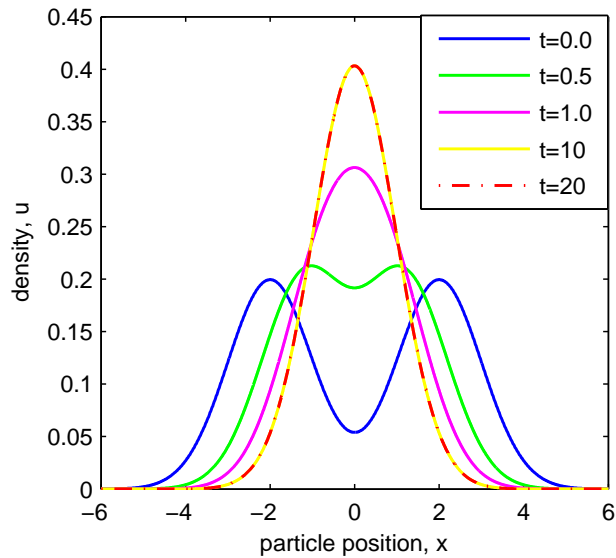


Figure 9: Evolution of density u with subcritical mass $M = 1$ and $\beta = 1$ ($h = 1/1000$, $\tau = 1/1000$, $m = 2$) in **Example 4**.

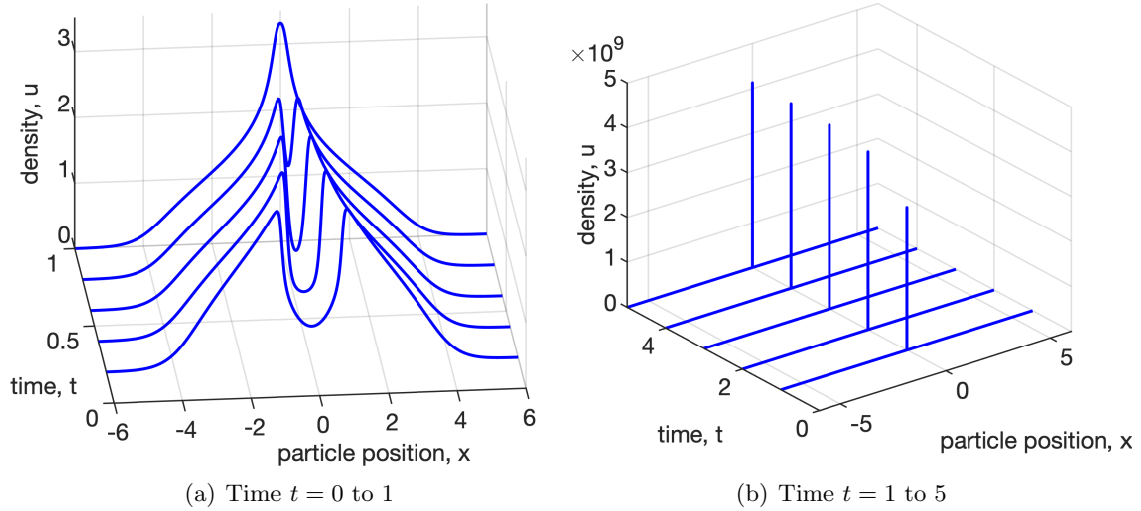


Figure 10: The evolution of density u with supercritical mass $M = 10$ in **Example 4** ($h = 1/1000$, $\tau = 1/10000$, $m = 2$).

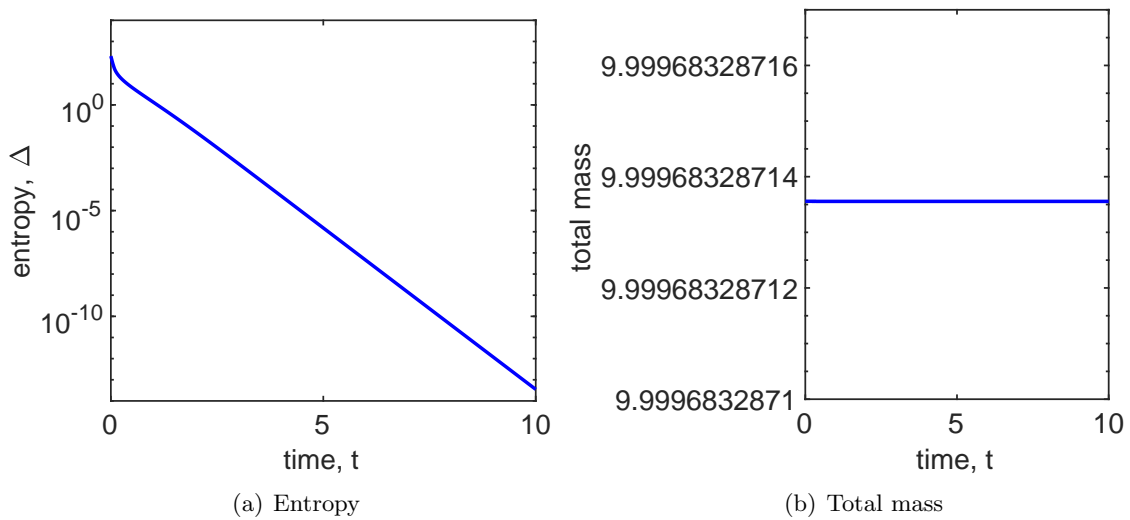
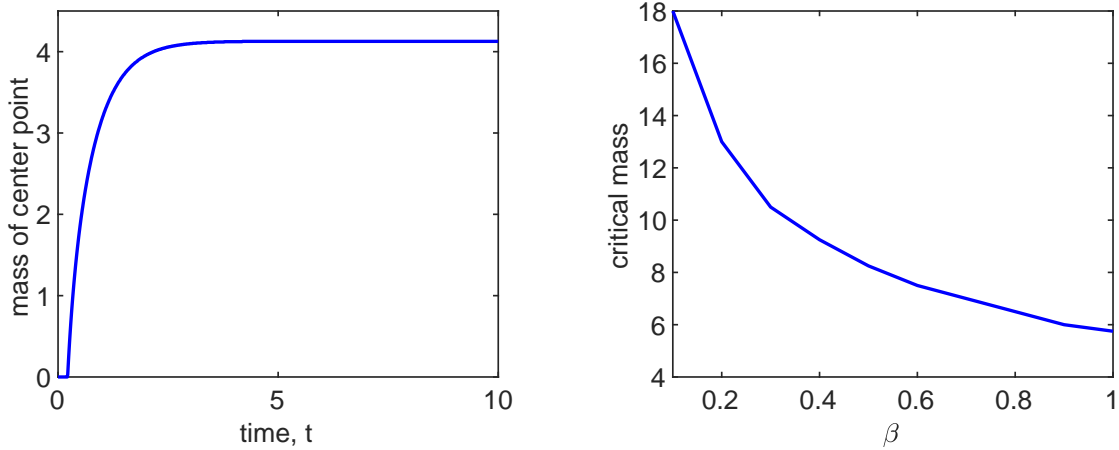


Figure 11: The evolution of entropy and total mass with subcritical mass $M = 10$ and $\beta = 1$ in **Example 4** ($h = 1/1000$, $\tau = 1/10000$, $m = 2$).



(a) Mass at the central point

(b) The relationship between β and the critical mass

Figure 12: The evolution of mass at central point ($\beta = 1$) and the critical mass with different β with subcritical mass $M = 10$ in **Example 4** ($h = 1/1000$, $\tau = 1/10000$, $m = 2$).

some conditions, there exists a unique steady state with a compact support. Moreover, the steady solution is a minimizer of a total energy [5]. In [48] and [3], the authors verified the above results with a discontinuous Galerkin method and finite volume schemes, respectively.

Example 5: Gaussian Interaction Kernel

In this example, we solve the Fokker–Planck equations

$$\partial_t u = \partial_x [u \partial_x (\nu u^{m-1} + W * u)], \quad x \in [-6, 6], \quad (5.13)$$

with a Gaussian kernel $W(x) = -\frac{1}{\sqrt{2\pi\sigma^2}} e^{-\frac{|x|^2}{2\sigma^2}}$, $\sigma > 0$, and the same initial condition as in [48]:

$$u(x, 0) = \frac{1}{2\sqrt{2\pi}} \left[e^{-\frac{(x-\frac{5}{2})^2}{2}} + e^{-\frac{(x+\frac{5}{2})^2}{2}} \right].$$

We split the Gaussian kernel W as follows:

$$W = W_c - W_e,$$

where

$$W_c = ax^2,$$

and

$$W_e = \frac{1}{\sqrt{2\pi\sigma^2}} e^{-\frac{|x|^2}{2\sigma^2} + ax^2},$$

with

$$a = \frac{1}{\sigma^2 \sqrt{2\pi\sigma^2}} \max \left\{ 1, e^{-\frac{l^2}{2\sigma^2}} \left(1 - \frac{l^2}{\sigma^2} \right) \right\}.$$

Notice that both W_c and W_e are convex functions.

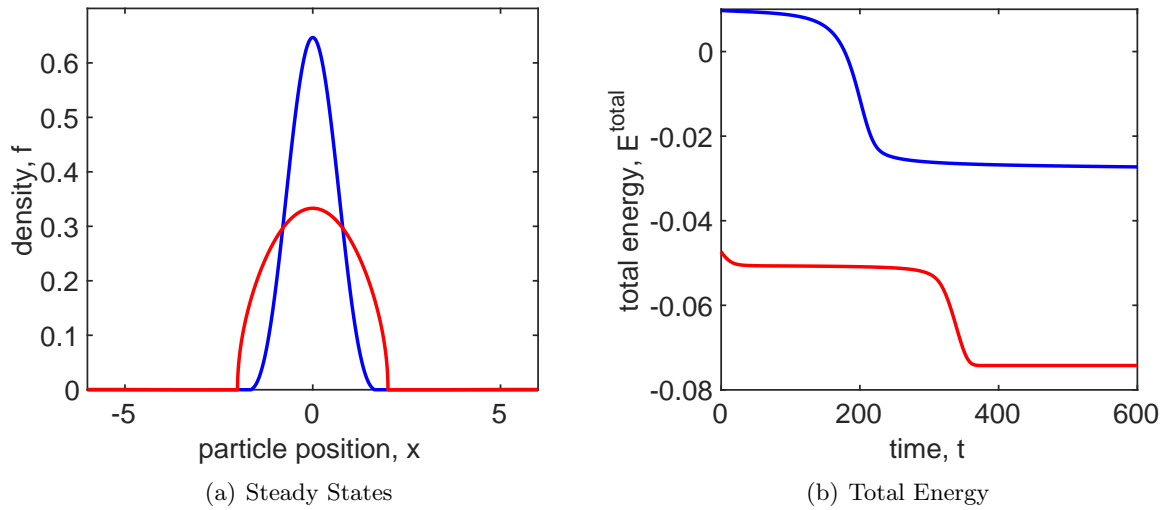


Figure 13: Steady-state solutions and the evolution of the total energy with $m = 1.5, \nu = 1.28$ (the blue line) and $m = 3, \nu = 0.28$ (the red line) in **Example 5** ($h = 1/100, \tau = 1/100$).

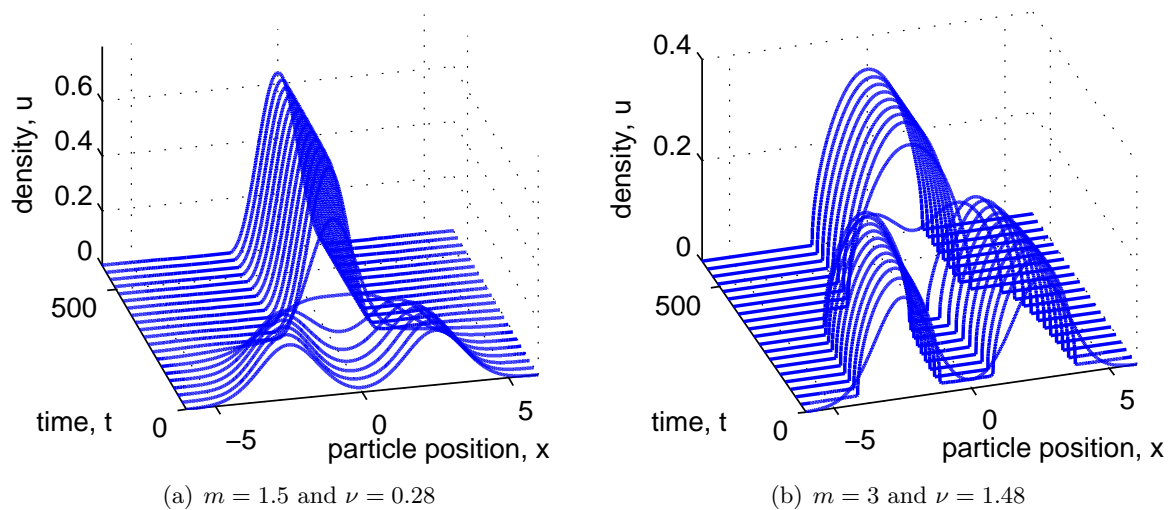


Figure 14: Evolution of the density u in **Example 5** ($h = 1/100, \tau = 1/100$)

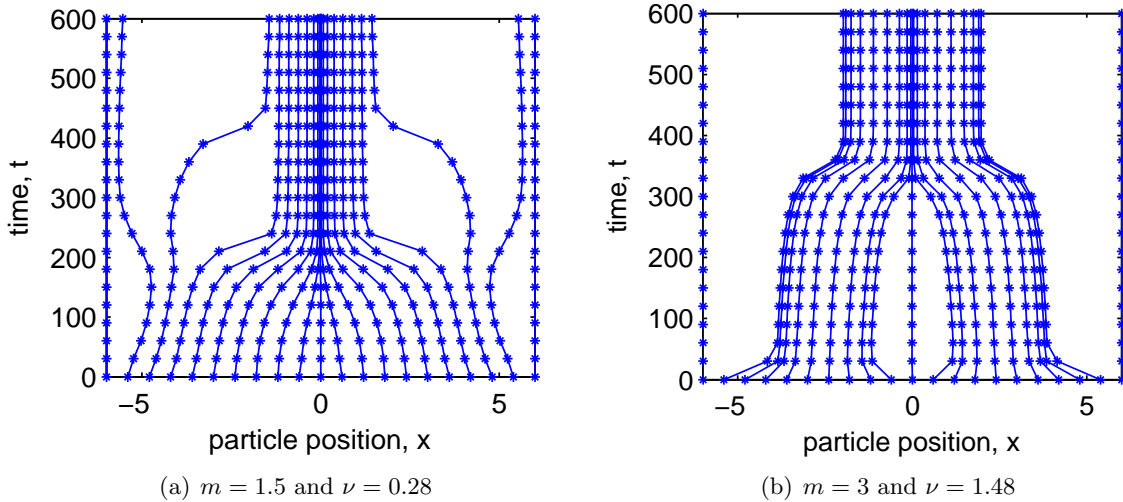


Figure 15: Particle trajectories in **Example 5** ($h = 1/100$, $\tau = 1/100$)

| h | τ | $\ e_h^u\ _2$ | Order | $\ e_h^u\ _\infty$ | Order |
|------|--------|---------------|-------|--------------------|-------|
| 1/10 | 1/10 | 7.880e-05 | | 5.158e-05 | |
| 1/20 | 1/40 | 1.985e-05 | 1.988 | 1.332e-05 | 1.953 |
| 1/40 | 1/160 | 4.098e-06 | 2.276 | 2.992e-06 | 2.155 |
| h | τ | $\ e_h^x\ _2$ | Order | $\ e_h^x\ _\infty$ | Order |
| 1/10 | 1/10 | 6.291e-04 | | 6.778e-04 | |
| 1/20 | 1/40 | 1.632e-04 | 1.953 | 1.767e-04 | 1.939 |
| 1/40 | 1/160 | 3.760e-05 | 2.155 | 4.177e-05 | 2.081 |

Table 4: Numerical error and convergence order of the numerical trajectory x and density u with $m = 1.5$ and $\nu = 0.28$ at time $t = 1$ in **Example 5**.

We solve the problem up to time $T = 1800$, at which the system almost reaches the steady state with $\sigma = 1$. Fig. 13 (a) shows the steady-state densities with compact supports for the cases with $m = 1.5, \nu = 0.28$ and $m = 3, \nu = 1.48$. We observe that the support gets larger as m increases. Fig. 13 (b) shows that the total energy decays slowly in the first stage and then decays sharply after certain critical time, especially for the case with $m = 3$. Similar results have been reported in the work [48], mainly due to the appearance of metastability. Fig. 14 (a) and (b) present the evolution of densities for $m = 1.5$ and $m = 3$, respectively. In comparison with the case of $m = 1.5$, the initial two smooth peaks quickly turn to two sharp bumps staying away from each other for $m = 3$. As the bumps get closer, the solution develops one support and grows up to a steady state. However, with $m = 1.5$, the initial two peaks merge into one smooth peak and subsequently go to the corresponding steady state. Fig. 15 (a) and (b) show the motion of particles for $m = 1.5, \nu = 0.28$ and $m = 3, \nu = 1.48$, respectively. For the case of $m = 1.5, \nu = 0.28$, most of the particles gradually move to the origin, developing a density bump at the origin. For $m = 3, \nu = 1.48$, in contrast, the particles first concentrate and develop

two density bumps, and subsequently move towards the origin. We also study the numerical accuracy of our schemes with the presence of nonlocal interactions. Table 4 shows that the error of numerical solution u and trajectory x with $m = 1.5$ and $\nu = 0.28$ at time $t = 1$ in \mathcal{L}^2 and \mathcal{L}^∞ norms. The reference exact solution is obtained numerically on a rather refined mesh with $h = 1/1000$ and $\tau = 1/1000$. The results reveal that our numerical method is second-order accurate in space and first-order accurate in time.

Remark 5.2. *The numerical simulations reveal a multi-phase convergence to equilibrium rather than a fixed-rate convergence, reminiscent of metastability. Intermediate aggregations that depend on the initial data can quickly form, even though the final steady state is simply connected and compactly supported. These aggregations eventually merge with an arbitrarily slow convergence rate, if the parameter σ is small [3, 48].*

6 Conclusions

In this work, we have proposed novel structure-preserving numerical schemes, based on the Energetic Variational Approach, to robustly solve the nonlinear Fokker–Planck equations with nonlocal interactions. The trajectory equation has been obtained by using the balance between the maximal dissipation principle and least action principle. With a convex-splitting technique, we have established numerical schemes that are uniquely solvable, with their numerical solutions satisfying the discrete energy dissipation law. Moreover, it has been proved that the developed numerical schemes can preserve mass conservation and positivity of solutions at fully discrete level. Numerical accuracy of second order in space and first order in time can be theoretically justified with detailed numerical analysis.

Numerical simulations have demonstrated several valuable features of the proposed schemes. In addition to the preservation of physical structures, such as positivity, conservation, discrete energy dissipation, and steady states, numerical tests have revealed that the developed numerical schemes are able to effectively and robustly solve degenerate cases of the Fokker–Planck equations with nonlocal interactions. For instance, our numerical schemes have been shown to have convergence order in degenerate cases in the presence of solutions with compact support, accurately calculate the waiting time of free boundaries without any oscillation, and approximate blow-up singularity with machine precision.

We now discuss several issues and possible further refinements of our work. Our numerical method has been proved to be second-order accurate in space and first-order accurate in time. It is desirable but challenging to develop second-order accurate temporal discretization that is able to preserve unconditional energy dissipation in the discrete sense. One promising idea is to employ the BDF discretization with an artificial Douglas-Dupont regularization term, which is added to ensure the energy dissipation [21]. Another improvement is to develop numerical methods and analysis to address a non-smooth (even singular) interaction kernel $W(\cdot)$. One possible strategy is to split the kernel into a smooth part and a non-smooth part that can be treated analytically. Finally, one limitation of this work is associated with the one-dimensional nature of the problem. In higher dimensions, the trajectory equation will be a very complicated nonlinear parabolic system with the Jacobian of the flow map in the denominator. The development of numerical schemes with structure-preserving properties for higher dimensional cases deserves further investigation.

Acknowledgments

The authors would like to thank anonymous reviewers for their helpful suggestions which lead to improvement of the work. C. Duan was supported in part by NSFC under the grant 11901109. C. Liu was partially supported by the United States-Israel Binational Science Foundation (BSF) # 2024246, and NSF grants DMS-1216938 and DMS-1418689. W. Chen was supported by the National Science Foundation of China (11671098) and partially supported by Shanghai science and technology research program (19JC1420101). W. Chen also thanks Institute of Scientific computation and Financial Data Analysis, Shanghai University of Finance and Economics for the support during his visit. X. Yue was partially supported by NSFC under the grant 11971342. S. Zhou was supported by the grants NSFC 21773165, Young Elite Scientist Sponsorship Program by Jiangsu Association For Science and Technology, and National Key R&D Program of China (No. 2018YFB0204404).

Reference

- [1] N. B. Abdallah, I. M. Gamba, G. Toscani, On the minimization problem of sub-linear convex functionals, *Kinet. Relat. Models* 4(4) (2011) 857-871.
- [2] D. G. Aronson, L. A. Caffarelli, S. Kamin, How an initially stationary interface begins to move in porous medium flow, *SIAM J. Math. Anal.* 14(4) (1983) 639-658.
- [3] R. Bailo, J. A. Carrillo, J. Hu, Fully discrete positivity-preserving and energy-decaying schemes for aggregation-diffusion equations with a gradient flow structure, arXiv preprint (2018) arXiv:1811.11502.
- [4] J. Barré, P. Degond, E. Zatorska, Kinetic theory of particle interactions mediated by dynamical networks, *Multiscale Model. Simul.* 15(3) (2017) 1294-1323.
- [5] J. Bedrossian, Global minimizers for free energies of subcritical aggregation equations with degenerate diffusion, *Appl. Math. Lett.* 24(11) (2011) 1927-1932.
- [6] D. Benedetto, E. Caglioti, J. A. Carrillo, M. Pulvirenti, A non-Maxwellian steady distribution for one-dimensional granular media, *J. Stat. Phys.* 91 (1998) 979-990.
- [7] M. Bessemoulin-Chatard, F. Filbet, A finite volume scheme for nonlinear degenerate parabolic equations, *SIAM J. Sci. Comput.* 34(5) (2012) B559-B583.
- [8] S. Boscarino, F. Filbet, G. Russo, High Order Semi-implicit Schemes for Time Dependent Partial Differential Equations, *J. Sci. Comput.* 68 (2016) 975-1001.
- [9] C. Buet, S. Cordier, and V. Dos Santos, A conservative and entropy scheme for a simplified model of granular media, *Transport Theor. Stat.* 33(2) (2004) 125-155.
- [10] M. Burger, R. Fetecau, Y. Huang, Stationary states and asymptotic behavior of aggregation models with nonlinear local repulsion, *SIAM J. Appl. Dyn. Syst.* 13(1) (2014) 397-424.
- [11] M. Burger, V. Capasso, D. Morale, On an aggregation model with long and short range interactions, *Nonlinear Anal. Real World Appl.* 8(3) (2007) 939-958.

- [12] J. A. Carrillo, A. Jüngel, P. A. Markowich, G. Toscani, A. Unterreiter, Entropy dissipation methods for degenerate parabolic problems and generalized Sobolev inequalities, *Monatshefte Math.* 133(1) (2001) 1-82.
- [13] J. A. Carrillo, G. Toscani, Asymptotic L^1 -decay of solutions of the porous medium equation to self-similarity, *Indiana Univ. Math. J.* 49(1) (2000) 113-142.
- [14] J. A. Carrillo, R. J. McCann, C. Villani, Kinetic equilibration rates for granular media and related equations: entropy dissipation and mass transportation estimates, *Rev. Mat. Iberoam.* 19(3) (2003) 971-1018.
- [15] J. A. Carrillo, Y. Huang, S. Martin, Explicit flock solutions for Quasi-Morse potentials, *Eur. J. Appl. Math.*, 25(5) (2014) 553-578.
- [16] J. A. Carrillo, M. Fornasier, G. Toscani, F. Vecil, Particle, kinetic, and hydrodynamic models of swarming. In *Mathematical modeling of collective behavior in socio-economic and life sciences*, *Model. Simul. Sci. Eng. Technol.*, pages 297-336. Birkhäuser Boston, Inc., Boston, MA, 2010.
- [17] J. A. Carrillo, A. Chertock, Y. Huang, A finite-volume method for nonlinear nonlocal equations with a gradient flow structure, *Commun. Comput. Phys.* 17 (2015) 233-258.
- [18] J. A. Carrillo, H. Ranetbauer, M. T. Wolfram, Numerical simulation of nonlinear continuity equations by evolving diffeomorphisms, *J. Comput. Phys.* 327 (2016) 186-202.
- [19] J. A. Carrillo, Y. Huang, F. S. Patacchini, G. Wolansky, Numerical study of a particle method for gradient flows, *Kinet. Relat. Models* 10(3) (2017) 613-641.
- [20] J. A. Carrillo, K. Craig, Y. Yao, Aggregation-diffusion equations: dynamics, asymptotics, and singular limits, *arXiv preprint arXiv:1810.03634*, 2018.
- [21] W. Chen, C. Wang, X. Wang, and S. M. Wise, Positivity-preserving, energy stable numerical schemes for the Cahn–Hilliard equation with logarithmic potential, *J. Comput. Phys.:X* 3 (2019) 100031.
- [22] Q. Du, C. Liu, R. Ryham, X. Wang, Energetic variational approaches in modeling vesicle and fluid interactions, *Phys. D* 238 (2009) 923-930.
- [23] C. Duan, C. Liu, C. Wang, X. Yue, Numerical complete solution for random genetic drift by Energetic Variational approach, *ESAIM: Math. Model. Num.* 53(2) (2019) 615-634.
- [24] C. Duan, C. Liu, C. Wang, X. Yue, Numerical methods for Porous Medium Equation by an Energetic Variational Approach, *J. Comput. Phys.* 385 (2019) 13-32.
- [25] C. Duan, C. Liu, C. Wang, X. Yue, Convergence Analysis of a Numerical Scheme for the Porous Medium Equation by an Energetic Variational Approach, *Numer. Math. Theor. Meth. Appl.* 13 (2020).
- [26] C. Duan, W. Chen, C. Liu, C. Wang, X. Yue, A second order accurate numerical scheme for the porous medium equation by an energetic variational approach, *arXiv preprint arXiv:2006.12354* (2020).

- [27] W. E, J. G. Liu, Projection method I: convergence and numerical boundary layers, *SIAM J. Numer. Anal.* 32 (1995) 1017-1057.
- [28] B. Eisenberg, Y. K. Hyon, C. Liu, Energy variational analysis of ions in water and channels: Field theory for primitive models of complex ionic fluids, *J. Chem. Phys.* 133(10) (2010) 104.
- [29] D. J. Eyre, Unconditionally gradient stable time marching the Cahn-Hilliard equation, in *MRS Proceedings*, Cambridge Univ. Press 529 (1998) 39.
- [30] Y. Hyon, D. Y. Kwak, C. Liu, Energetic variational approach in complex fluids: maximum dissipation principle, *Discrete Contin. Dyn. Syst.* 26(4) (2010) 1291-1304.
- [31] H. Koba, C. Liu, Y. Giga, Energetic variational approaches for incompressible fluid systems on an evolving surface, *Quart. Appl. Math.* 75 (2017) 359-389.
- [32] T. Kolokolnikov, J. A. Carrillo, A. Bertozzi, R. Fetecau, and M. Lewis. Emergent behaviour in multi-particle systems with non-local interactions [Editorial], *Phys. D* 260 (2013) 1-4.
- [33] C. Liu, J. Shen, A phase field model for the mixture of two incompressible fluids and its approximation by a Fourier-spectral method, *Phys. D* 179(3-4) (2003) 211-228.
- [34] C. Liu, H. Wu, An energetic variational approach for the Cahn-Hilliard equation with dynamic boundary conditions, *Arch. Ration. Mech. Anal.* 233(1) (2019) 167-247.
- [35] H. Liu, Z. Wang, An entropy satisfying discontinuous Galerkin method for nonlinear Fokker-Planck equations, *J. Sci. Comput.* 68(3) (2016) 1217-1240.
- [36] H. Liu, Z. Wang, A free energy satisfying discontinuous Galerkin method for one-dimensional Poisson-Nernst-Planck systems, *J. Comput. Phys.* 328 (2017) 413-437.
- [37] P. M. Lushnikov, N. Chen, M. Alber, Macroscopic dynamics of biological cells interacting via chemotaxis and direct contact, *Phys. Rev. E* 78 (2008) 061904.
- [38] Y. Nesterov, A. Nemirovskii, Interior-point polynomial algorithms in convex programming, SIAM, 1994.
- [39] L. Onsager, Reciprocal relations in irreversible processes, *Phys. Rev. II. Ser.* 38 (1931) 2265-2279.
- [40] L. Onsager, Reciprocal relations in irreversible processes, *Phys. Rev. I.* 37(4) (1931) 405.
- [41] L. Pareschi, M. Zanella, Structure Preserving Schemes for Nonlinear Fokker-Planck Equations and Applications, *J. Sci. Comput.* 73(3) (2017) 1575-1600.
- [42] Y. Qian, Z. Wang, S. Zhou, A conservative, free energy dissipating, and positivity preserving finite difference scheme for multi-dimensional nonlocal Fokker-Planck equation, *J. Comput. Phys.* 386 (1) (2019) 22-36.
- [43] H. Liu, Z. Wang, A free energy satisfying discontinuous Galerkin method for one-dimensional Poisson-Nernst-Planck systems, *J. Comput. Phys.* 328 (2017) 413-437.

- [44] H. Liu, Z. Wang, A free energy satisfying finite difference method for Poisson–Nernst–Planck equations, *J. Comput. Phys.* 268 (2014) 363-376.
- [45] M. S. Metti, J. Xu, C. Liu, Energetically stable discretizations for charge transport and electrokinetic models, *J. Comput. Phys.* 306 (2016) 1-18.
- [46] J. Ding, Z. Wang, S. Zhou, Positivity preserving finite difference methods for Poisson–Nernst–Planck equations with steric interactions: Application to slit-shaped nanopore conductance, *J. Comput. Phys.* 397 (2019) 108864.
- [47] J. W. Strutt, Some general theorems relating to vibrations, *P. Lond. Math. Soc.* IV (1873) 357-368.
- [48] Z. Sun, J. A. Carrillo, C.-W. Shu, A discontinuous Galerkin method for nonlinear parabolic equations and gradient flow problems with interaction potentials, *J. Comput. Phys.* 352 (2018) 76-104.
- [49] C. M. Topaz, A. L. Bertozzi, M. A. Lewis, A nonlocal continuum model for biological aggregation, *Bull. Math. Biol.* 68 (2006) 1601-1623.
- [50] J. L. Vázquez, *The Porous Medium Equation*, Oxford University Press, Oxford, 2007.
- [51] C. Villani, *Topics in Optimal Transportation*, American Mathematical Society, 2003.
- [52] C. Wang, J. G. Liu, Convergence of gauge method for incompressible flow, *Math. Comp.* 69 (2000) 1385-1407.